HALF-SPACE IMPEDANCE LAPLACE PROBLEM

4.1 Introduction

In this chapter we study the perturbed half-space impedance Laplace problem using integral equation techniques and the boundary element method.

We consider the problem of the Laplace equation in three dimensions on a compactly perturbed half-space with an impedance boundary condition. The perturbed half-space impedance Laplace problem is a surface wave scattering problem around the bounded perturbation, which is contained in the upper half-space. In water-wave scattering the impedance boundary-value problem appears as a consequence of the linearized free-surface condition, which allows the propagation of surface waves (vid. Section A.10). This problem can be regarded as a limit case when the frequency of the volume waves, i.e., the wave number in the Helmholtz equation, tends towards zero (vid. Chapter V). The two-dimensional case is considered in Chapter II, whereas the full-space impedance Laplace problem with a bounded impenetrable obstacle is treated thoroughly in Appendix D.

The main application of the problem corresponds to linear water-wave propagation in a liquid of indefinite depth, which was first studied in the classical works of Cauchy (1827) and Poisson (1818). A study of wave motion caused by a submerged obstacle was carried out by Lamb (1916). The major impulse in the field came after the milestone papers on the motion of floating bodies by John (1949, 1950), who considered a Green's function and integral equations to solve the problem. Another expression for the Green's function was suggested by Havelock (1955), which was later rederived or publicized in different forms by Kim (1965), Hearn (1977), Noblesse (1982), and Newman (1984*b*, 1985), Pidcock (1985), and Chakrabarti (2001). Other expressions for this Green's function can be found in the articles of Moran (1964), Hess & Smith (1967), and Peter & Meylan (2004), and likewise in the books of Dautray & Lions (1987) and Duffy (2001). The main references for the problem are the classical article of Wehausen & Laitone (1960) and the books of Mei (1983), Linton & McIver (2001), Kuznetsov, Maz'ya & Vainberg (2002), and Mei, Stiassnie & Yue (2005). Reviews of the numerical methods used to solve water-wave problems can be found in Mei (1978) and Yeung (1982).

The Laplace equation does not allow the propagation of volume waves inside the considered domain, but the addition of an impedance boundary condition permits the propagation of surface waves along the boundary of the perturbed half-space. The main difficulty in the numerical treatment and resolution of our problem is the fact that the exterior domain is unbounded. We solve it therefore with integral equation techniques and a boundary element method, which require the knowledge of the associated Green's function. This Green's function is computed using a Fourier transform and taking into account the limiting absorption principle, following Durán, Muga & Nédélec (2005*b*, 2009), but here an explicit expression is found for it in terms of a finite combination of elementary functions, special functions, and their primitives.

This chapter is structured in 13 sections, including this introduction. The direct scattering problem of the Laplace equation in a three-dimensional compactly perturbed half-space with an impedance boundary condition is presented in Section 4.2. The computation of the Green's function, its far field, and its numerical evaluation are developed respectively in Sections 4.3, 4.4, and 4.5. The use of integral equation techniques to solve the direct scattering problem is discussed in Section 4.6. These techniques allow also to represent the far field of the solution, as shown in Section 4.7. The appropriate function spaces and some existence and uniqueness results for the solution of the problem are presented in Section 4.8. The dissipative problem is studied in Section 4.9. By means of the variational formulation developed in Section 4.10, the obtained integral equation is discretized using the boundary element method, which is described in Section 4.11. The boundary element calculations required to build the matrix of the linear system resulting from the numerical discretization are explained in Section 4.12. Finally, in Section 4.13 a benchmark problem based on an exterior half-sphere problem is solved numerically.

4.2 Direct scattering problem

4.2.1 Problem definition

We consider the direct scattering problem of linear time-harmonic surface waves on a perturbed half-space $\Omega_e \subset \mathbb{R}^3_+$, where $\mathbb{R}^3_+ = \{(x_1, x_2, x_3) \in \mathbb{R}^3 : x_3 > 0\}$, where the incident field u_I is known, and where the time convention $e^{-i\omega t}$ is taken. The goal is to find the scattered field u as a solution to the Laplace equation in the exterior open and connected domain Ω_e, satisfying an outgoing surface-wave radiation condition, and such that the total field u_T, which is decomposed as $u_T = u_I + u$, satisfies a homogeneous impedance boundary condition on the regular boundary $\Gamma = \Gamma_p \cup \Gamma_\infty$ (e.g., of class C^2). The exterior domain Ω_e is composed by the half-space $\mathbb{R}^3_+$ with a compact perturbation near the origin that is contained in $\mathbb{R}^3_+$, as shown in Figure 4.1. The perturbed boundary is denoted by Γ_p, while Γ_∞ denotes the remaining unperturbed boundary of $\mathbb{R}^3_+$, which extends towards infinity on every horizontal direction. The unit normal $\boldsymbol{n}$ is taken outwardly oriented of Ω_e and the complementary domain is denoted by $\Omega_c = \mathbb{R}^3 \setminus \overline{\Omega_e}$.

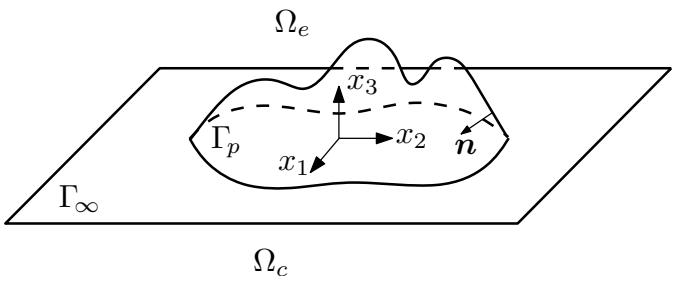

FIGURE 4.1. Perturbed half-space impedance Laplace problem domain.

The total field u_T satisfies thus the Laplace equation

$$\Delta u_T = 0 \qquad \text{in } \Omega_e, \tag{4.1}$$

which is also satisfied by the incident field u_I and the scattered field u, due linearity. For the total field u_T we take the homogeneous impedance boundary condition

$$-\frac{\partial u_T}{\partial n} + Z u_T = 0 \qquad \text{on } \Gamma, \tag{4.2}$$

where Z is the impedance on the boundary, which is decomposed as

$$Z(\boldsymbol{x}) = Z_\infty + Z_p(\boldsymbol{x}), \qquad \boldsymbol{x} \in \Gamma, \tag{4.3}$$

being $Z_\infty > 0$ real and constant throughout Γ, and $Z_p(\boldsymbol{x})$ a possibly complex-valued impedance that depends on the position $\boldsymbol{x}$ and that has a bounded support contained in Γ_p. The case of a complex Z_∞ will be discussed later. For linear water waves, the free-surface condition considers $Z_\infty = \omega^2/g$, where ω is the radian frequency or pulsation and g denotes the acceleration caused by gravity. If $Z = 0$ or $Z = \infty$, then we retrieve respectively the classical Neumann or Dirichlet boundary conditions. The scattered field u satisfies the non-homogeneous impedance boundary condition

$$-\frac{\partial u}{\partial n} + Z u = f_z \qquad \text{on } \Gamma, \tag{4.4}$$

where the impedance data function f_z is known, has its support contained in Γ_p, and is given, because of (4.2), by

$$f_z = \frac{\partial u_I}{\partial n} - Z u_I \qquad \text{on } \Gamma. \tag{4.5}$$

An outgoing surface-wave radiation condition has to be also imposed for the scattered field u, which specifies its decaying behavior at infinity and eliminates the non-physical solutions, e.g., ingoing surface waves or exponential growth inside Ω_e. This radiation condition can be stated for $r \to \infty$ in a more adjusted way as

$$\begin{cases} |u| \le \dfrac{C}{r^2} \quad \text{and} \quad \left|\dfrac{\partial u}{\partial r}\right| \le \dfrac{C}{r^3} & \text{if } x_3 > \dfrac{1}{2Z_\infty}\ln\bigl(1 + 2\pi Z_\infty r^3\bigr), \\[2ex] |u| \le \dfrac{C}{\sqrt{r}} \quad \text{and} \quad \left|\dfrac{\partial u}{\partial r} - iZ_\infty u\right| \le \dfrac{C}{r} & \text{if } x_3 \le \dfrac{1}{2Z_\infty}\ln\bigl(1 + 2\pi Z_\infty r^3\bigr), \end{cases} \tag{4.6}$$

for some constants $C > 0$, where $r = |\boldsymbol{x}|$. It implies that two different asymptotic behaviors can be established for the scattered field u. Away from the boundary Γ and inside the domain Ω_e, the first expression in (4.6) dominates, which is related to the asymptotic decaying condition (D.5) of the Laplace equation on the exterior of a bounded obstacle. Near the boundary, on the other hand, the second part of the second expression in (4.6) resembles a Sommerfeld radiation condition like (E.8), but only along the boundary, and is therefore related to the propagation of surface waves. It is often expressed also as

$$\left|\frac{\partial u}{\partial |\boldsymbol{x}_s|} - iZ_\infty u\right| \le \frac{C}{|\boldsymbol{x}_s|}, \tag{4.7}$$

where $\boldsymbol{x}_s = (x_1, x_2)$.

Analogously as done by Durán, Muga & Nédélec (2005*b*, 2009) for the Helmholtz equation, the radiation condition (4.6) can be stated alternatively as

$$\begin{cases} |u| \leq \dfrac{C}{r^{2-2\alpha}} \quad \text{and} \quad \left|\dfrac{\partial u}{\partial r}\right| \leq \dfrac{C}{r^{3-2\alpha}} & \text{if } \ x_3 > Cr^{\alpha}, \\ |u| \leq \dfrac{C}{\sqrt{r}} \quad \text{and} \quad \left|\dfrac{\partial u}{\partial r} - iZ_{\infty}u\right| \leq \dfrac{C}{r^{1-\alpha}} & \text{if } \ x_3 \leq Cr^{\alpha}, \end{cases} \tag{4.8}$$

for $0 < \alpha < 1/2$ and some constants $C > 0$, being the growth of Cr^{α} bigger than the logarithmic one at infinity. Equivalently, the radiation condition can be expressed in a more weaker and general formulation as

$$\begin{cases} \lim\limits_{R\to\infty} \displaystyle\int_{S_R^1} |u|^2 \, \mathrm{d}\gamma = 0 \quad \text{and} \quad \lim\limits_{R\to\infty} \displaystyle\int_{S_R^1} R^2 \left|\frac{\partial u}{\partial r}\right|^2 \mathrm{d}\gamma = 0, \\ \lim\limits_{R\to\infty} \displaystyle\int_{S_R^2} \frac{|u|^2}{\ln R} \, \mathrm{d}\gamma < \infty \quad \text{and} \quad \lim\limits_{R\to\infty} \displaystyle\int_{S_R^2} \frac{1}{\ln R} \left|\frac{\partial u}{\partial r} - iZ_{\infty}u\right|^2 \mathrm{d}\gamma = 0, \end{cases} \tag{4.9}$$

where

$$S_R^1 = \left\{ \boldsymbol{x} \in \mathbb{R}^3_+ : \, |\boldsymbol{x}| = R, \ \ x_3 > \frac{1}{2Z_{\infty}} \ln\bigl(1 + 2\pi Z_{\infty} R^3\bigr) \right\}, \tag{4.10}$$

$$S_R^2 = \left\{ \boldsymbol{x} \in \mathbb{R}^3_+ : \, |\boldsymbol{x}| = R, \ \ x_3 < \frac{1}{2Z_{\infty}} \ln\bigl(1 + 2\pi Z_{\infty} R^3\bigr) \right\}. \tag{4.11}$$

We observe that in this case

$$\int_{S_R^1} \mathrm{d}\gamma = \mathcal{O}(R^2) \qquad \text{and} \qquad \int_{S_R^2} \mathrm{d}\gamma = \mathcal{O}(R \ln R). \tag{4.12}$$

The portions S_R^1 and S_R^2 of the half-sphere and the terms depending on S_R^2 of the radiation condition (4.9) have to be modified when using instead the polynomial curves of (4.8). We refer to Stoker (1956) for a discussion on radiation conditions for surface waves.

The perturbed half-space impedance Laplace problem can be finally stated as

$$\begin{cases} \text{Find } u : \Omega_e \to \mathbb{C} \text{ such that} \\ \Delta u = 0 & \text{in } \ \Omega_e, \\ -\dfrac{\partial u}{\partial n} + Zu = f_z & \text{on } \ \Gamma, \\ \text{+ Outgoing radiation condition as } |\boldsymbol{x}| \to \infty, \end{cases} \tag{4.13}$$

where the outgoing radiation condition is given by (4.6).

4.2.2 Incident field

To determine the incident field u_I, we study the solutions of the unperturbed and homogeneous wave propagation problem with neither a scattered field nor an associated radiation condition. The solutions are searched in particular to be physically admissible, i.e., solutions which do not explode exponentially in the propagation domain, depicted in Figure 4.2.

We analyze thus the half-space impedance Laplace problem

$$\begin{cases} \Delta u_I = 0 & \text{in } \mathbb{R}^3_+, \\ \dfrac{\partial u_I}{\partial x_3} + Z_\infty u_I = 0 & \text{on } \{x_3 = 0\}. \end{cases} \tag{4.14}$$

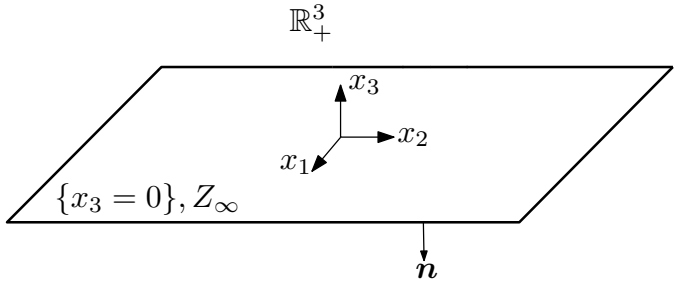

FIGURE 4.2. Positive half-space $\mathbb{R}^3_+$.

The solutions u_I of the problem (4.14) are given, up to an arbitrary scaling factor, by the progressive plane surface waves

$$u_I(\boldsymbol{x}) = e^{i\boldsymbol{k}_s \cdot \boldsymbol{x}_s} e^{-Z_\infty x_3}, \qquad (\boldsymbol{k}_s \cdot \boldsymbol{k}_s) = Z_\infty^2, \qquad \boldsymbol{x}_s = (x_1, x_2). \tag{4.15}$$

They correspond to progressive plane volume waves of the form $e^{i\boldsymbol{k}\cdot\boldsymbol{x}}$ with a complex wave propagation vector $\boldsymbol{k} = (\boldsymbol{k}_s, iZ_\infty)$, where $\boldsymbol{k}_s \in \mathbb{R}^2$. It can be observed that these surface waves are guided along the half-space's boundary, and decrease exponentially towards its interior, hence their name. They vanish completely for classical Dirichlet ($Z_\infty = \infty$) or Neumann ($Z_\infty = 0$) boundary conditions.

4.3 Green's function

4.3.1 Problem definition

The Green's function represents the response of the unperturbed system to a Dirac mass. It corresponds to a function G, which depends on the impedance Z_∞, on a fixed source point $\boldsymbol{x} \in \mathbb{R}^3_+$, and on an observation point $\boldsymbol{y} \in \mathbb{R}^3_+$. The Green's function is computed in the sense of distributions for the variable $\boldsymbol{y}$ in the half-space $\mathbb{R}^3_+$ by placing at the right-hand side of the Laplace equation a Dirac mass $\delta_{\boldsymbol{x}}$, centered at the point $\boldsymbol{x}$. It is therefore a solution for the radiation problem of a point source, namely

$$\begin{cases} \text{Find } G(\boldsymbol{x}, \cdot) : \mathbb{R}^3_+ \to \mathbb{C} \text{ such that} \\ \Delta_{\boldsymbol{y}} G(\boldsymbol{x}, \boldsymbol{y}) = \delta_{\boldsymbol{x}}(\boldsymbol{y}) & \text{in } \mathcal{D}'(\mathbb{R}^3_+), \\ \dfrac{\partial G}{\partial y_3}(\boldsymbol{x}, \boldsymbol{y}) + Z_\infty G(\boldsymbol{x}, \boldsymbol{y}) = 0 & \text{on } \{y_3 = 0\}, \\ \text{+ Outgoing radiation condition as } |\boldsymbol{y}| \to \infty. \end{cases} \tag{4.16}$$

The outgoing radiation condition, in the same way as in (4.6), is given here as $|\boldsymbol{y}| \to \infty$ by

$$\begin{cases} |G| \leq \dfrac{C}{|\boldsymbol{y}|^2} \quad \text{and} \quad \left|\dfrac{\partial G}{\partial r_{\boldsymbol{y}}}\right| \leq \dfrac{C}{|\boldsymbol{y}|^3} & \text{if } \; y_3 > \dfrac{\ln\bigl(1+2\pi Z_\infty |\boldsymbol{y}|^3\bigr)}{2Z_\infty}, \\ |G| \leq \dfrac{C}{\sqrt{|\boldsymbol{y}|}} \quad \text{and} \quad \left|\dfrac{\partial G}{\partial r_{\boldsymbol{y}}} - iZ_\infty G\right| \leq \dfrac{C}{|\boldsymbol{y}|} & \text{if } \; y_3 \leq \dfrac{\ln\bigl(1+2\pi Z_\infty |\boldsymbol{y}|^3\bigr)}{2Z_\infty}, \end{cases} \tag{4.17}$$

for some constants $C > 0$, which are independent of $r = |\boldsymbol{y}|$.

4.3.2 Special cases

When the Green's function problem (4.16) is solved using either homogeneous Dirichlet or Neumann boundary conditions, then its solution is found straightforwardly using the method of images (cf., e.g., Morse & Feshbach 1953).

a) Homogeneous Dirichlet boundary condition

We consider in the problem (4.16) the particular case of a homogeneous Dirichlet boundary condition, namely

$$G(\boldsymbol{x}, \boldsymbol{y}) = 0, \qquad \boldsymbol{y} \in \{y_3 = 0\}, \tag{4.18}$$

which corresponds to the limit case when the impedance is infinite ($Z_\infty = \infty$). In this case, the Green's function G can be explicitly calculated using the method of images, since it has to be antisymmetric with respect to the plane $\{y_3 = 0\}$. An additional image source point $\bar{\boldsymbol{x}} = (x_1, x_2, -x_3)$, located on the lower half-space and associated with a negative Dirac mass, is placed for this purpose just opposite to the upper half-space's source point $\boldsymbol{x} = (x_1, x_2, x_3)$. The desired solution is then obtained by evaluating the full-space Green's function (D.20) for each Dirac mass, which yields finally

$$G(\boldsymbol{x}, \boldsymbol{y}) = -\frac{1}{4\pi|\boldsymbol{y} - \boldsymbol{x}|} + \frac{1}{4\pi|\boldsymbol{y} - \bar{\boldsymbol{x}}|}. \tag{4.19}$$

b) Homogeneous Neumann boundary condition

We consider in the problem (4.16) the particular case of a homogeneous Neumann boundary condition, namely

$$\frac{\partial G}{\partial n_{\boldsymbol{y}}}(\boldsymbol{x}, \boldsymbol{y}) = 0, \qquad \boldsymbol{y} \in \{y_3 = 0\}, \tag{4.20}$$

which corresponds to the limit case when the impedance is zero ($Z_\infty = 0$). As in the previous case, the method of images is again employed, but now the half-space Green's function G has to be symmetric with respect to the plane $\{y_3 = 0\}$. Therefore, an additional image source point $\bar{\boldsymbol{x}} = (x_1, x_2, -x_3)$, located on the lower half-space, is placed just opposite to the upper half-space's source point $\boldsymbol{x} = (x_1, x_2, x_3)$, but now associated with a positive Dirac mass. The desired solution is then obtained by evaluating the full-space Green's function (D.20) for each Dirac mass, which yields

$$G(\boldsymbol{x}, \boldsymbol{y}) = -\frac{1}{4\pi|\boldsymbol{y} - \boldsymbol{x}|} - \frac{1}{4\pi|\boldsymbol{y} - \bar{\boldsymbol{x}}|}. \tag{4.21}$$

4.3.3 Spectral Green's function

a) Boundary-value problem

To solve (4.16) in the general case, we use a modified partial Fourier transform on the horizontal (y_1, y_2)-plane, taking advantage of the fact that there is no horizontal variation in the geometry of the problem. To obtain the corresponding spectral Green's function, we follow the same procedure as the one performed in Durán et al. (2005*b*). We define the forward Fourier transform of a function $F\big(\boldsymbol{x}, (\cdot, \cdot, y_3)\big) : \mathbb{R}^2 \to \mathbb{C}$ by

$$\widehat{F}(\boldsymbol{\xi}; y_3, x_3) = \frac{1}{2\pi} \int_{\mathbb{R}^2} F(\boldsymbol{x}, \boldsymbol{y})\, e^{-i\boldsymbol{\xi}\cdot(\boldsymbol{y}_s - \boldsymbol{x}_s)}\, \mathrm{d}\boldsymbol{y}_s, \qquad \boldsymbol{\xi} = (\xi_1, \xi_2) \in \mathbb{R}^2, \tag{4.22}$$

and its inverse by

$$F(\boldsymbol{x}, \boldsymbol{y}) = \frac{1}{2\pi} \int_{\mathbb{R}^2} \widehat{F}(\boldsymbol{\xi}; y_3, x_3)\, e^{i\boldsymbol{\xi}\cdot(\boldsymbol{y}_s - \boldsymbol{x}_s)}\, \mathrm{d}\boldsymbol{\xi}, \qquad \boldsymbol{y}_s = (y_1, y_2) \in \mathbb{R}^2, \tag{4.23}$$

where $\boldsymbol{x}_s = (x_1, x_2) \in \mathbb{R}^2$ and thus $\boldsymbol{x} = (\boldsymbol{x}_s, x_3)$.

To ensure a correct integration path for the Fourier transform and correct physical results, the calculations have to be performed in the framework of the limiting absorption principle, which allows to treat all the appearing integrals as Cauchy principal values. For this purpose, we take a small dissipation parameter $\varepsilon > 0$ into account and consider the problem (4.16) as the limit case when $\varepsilon \to 0$ of the dissipative problem

$$\begin{cases} \text{Find } G_\varepsilon(\boldsymbol{x}, \cdot) : \mathbb{R}^3_+ \to \mathbb{C} \text{ such that} & \\ \Delta_{\boldsymbol{y}} G_\varepsilon(\boldsymbol{x}, \boldsymbol{y}) = \delta_{\boldsymbol{x}}(\boldsymbol{y}) & \text{in } \mathcal{D}'(\mathbb{R}^3_+), \\ \dfrac{\partial G_\varepsilon}{\partial y_3}(\boldsymbol{x}, \boldsymbol{y}) + Z_\varepsilon G_\varepsilon(\boldsymbol{x}, \boldsymbol{y}) = 0 & \text{on } \{y_3 = 0\}, \end{cases} \tag{4.24}$$

where $Z_\varepsilon = Z_\infty + i\varepsilon$. This choice ensures a correct outgoing dissipative surface-wave behavior. Further references for the application of this principle can be found in Lenoir & Martin (1981) and in Hazard & Lenoir (1998).

Applying thus the Fourier transform (4.22) on the system (4.24) leads to a linear second order ordinary differential equation for the variable y_3, with prescribed boundary values, given by

$$\begin{cases} \dfrac{\partial^2 \widehat{G}_\varepsilon}{\partial y_3^2}(\boldsymbol{\xi}) - |\boldsymbol{\xi}|^2 \widehat{G}_\varepsilon(\boldsymbol{\xi}) = \dfrac{\delta(y_3 - x_3)}{2\pi}, & y_3 > 0, \\ \dfrac{\partial \widehat{G}_\varepsilon}{\partial y_3}(\boldsymbol{\xi}) + Z_\varepsilon \widehat{G}_\varepsilon(\boldsymbol{\xi}) = 0, & y_3 = 0. \end{cases} \tag{4.25}$$

To describe the (ξ_1, ξ_2)-plane, we use henceforth the system of signed polar coordinates

$$\xi = \begin{cases} \sqrt{\xi_1^2 + \xi_2^2} & \text{if } \xi_2 > 0, \\ \xi_1 & \text{if } \xi_2 = 0, \\ -\sqrt{\xi_1^2 + \xi_2^2} & \text{if } \xi_2 < 0, \end{cases} \qquad \text{and} \qquad \psi = \operatorname{arccot}\left(\frac{\xi_1}{\xi_2}\right), \tag{4.26}$$

where $-\infty < \xi < \infty$ and $0 \le \psi < \pi$. From (4.25) it is not difficult to see that the solution $\widehat{G}_\varepsilon$ depends only on $|\boldsymbol{\xi}|$, and therefore only on ξ, since $|\xi| = |\boldsymbol{\xi}|$. We remark that

the inverse Fourier transform (4.23) can be stated equivalently as

$$F(\boldsymbol{x},\boldsymbol{y}) = \frac{1}{2\pi}\int_{-\infty}^{\infty}\int_{0}^{\pi} \widehat{F}(\xi,\psi;y_3,x_3)|\xi|\, e^{i\xi\{(y_1-x_1)\cos\psi+(y_2-x_2)\sin\psi\}}\,\mathrm{d}\psi\,\mathrm{d}\xi. \tag{4.27}$$

We use the method of undetermined coefficients, and solve the homogeneous differential equation of the problem (4.25) respectively in the zone $\{\boldsymbol{y}\in\mathbb{R}^3_+ :\ 0<y_3<x_3\}$ and in the half-space $\{\boldsymbol{y}\in\mathbb{R}^3_+ :\ y_3>x_3\}$. This gives a solution for $\widehat{G}_\varepsilon$ in each domain, as a linear combination of two independent solutions of an ordinary differential equation, namely

$$\widehat{G}_\varepsilon(\xi) = \begin{cases} a\, e^{|\xi|y_3} + b\, e^{-|\xi|y_3} & \text{for } \ 0<y_3<x_3, \\ c\, e^{|\xi|y_3} + d\, e^{-|\xi|y_3} & \text{for } \ y_3>x_3. \end{cases} \tag{4.28}$$

The unknowns a, b, c, and d, which depend on ξ and x_3, are determined through the boundary condition, by imposing continuity, and by assuming an outgoing wave behavior.

b) Spectral Green's function with dissipation

Now, thanks to (4.28), the computation of $\widehat{G}_\varepsilon$ is straightforward. From the boundary condition of (4.25) a relation for the coefficients a and b can be derived, which is given by

$$a\big(Z_\varepsilon+|\xi|\big)+b\big(Z_\varepsilon-|\xi|\big)=0. \tag{4.29}$$

On the other hand, since the solution (4.28) has to be bounded at infinity as $y_3\to\infty$, it follows then necessarily that

$$c=0. \tag{4.30}$$

To ensure the continuity of the Green's function at the point $y_3=x_3$, it is needed that

$$d = a\, e^{|\xi|2x_3}+b. \tag{4.31}$$

Using relations (4.29), (4.30), and (4.31) in (4.28), we obtain the expression

$$\widehat{G}_\varepsilon(\xi) = a\, e^{|\xi|x_3}\left[e^{-|\xi||y_3-x_3|} - \left(\frac{Z_\varepsilon+|\xi|}{Z_\varepsilon-|\xi|}\right)e^{-|\xi|(y_3+x_3)}\right]. \tag{4.32}$$

The remaining unknown coefficient a is determined by replacing (4.32) in the differential equation of (4.25), taking the derivatives in the sense of distributions, particularly

$$\frac{\partial}{\partial y_3}\left\{e^{-|\xi||y_3-x_3|}\right\} = -|\xi|\,\mathrm{sign}(y_3-x_3)\, e^{-|\xi||y_3-x_3|}, \tag{4.33}$$

and

$$\frac{\partial}{\partial y_3}\big\{\mathrm{sign}(y_3-x_3)\big\} = 2\,\delta(y_3-x_3). \tag{4.34}$$

So, the second derivative of (4.32) becomes

$$\frac{\partial^2\widehat{G}_\varepsilon}{\partial y_3^2}(\xi) = a\, e^{|\xi|x_3}\left[|\xi|^2 e^{-|\xi||y_3-x_3|} - 2|\xi|\delta(y_3-x_3) - \left(\frac{Z_\varepsilon+|\xi|}{Z_\varepsilon-|\xi|}\right)|\xi|^2 e^{-|\xi|(y_3+x_3)}\right]. \tag{4.35}$$

This way, from (4.32) and (4.35) in the first equation of (4.25), we obtain that

$$a = -\frac{e^{-|\xi|x_3}}{4\pi|\xi|}. \tag{4.36}$$

Finally, the spectral Green's function $\widehat{G}_\varepsilon$ with dissipation ε is given by

$$\widehat{G}_\varepsilon(\xi; y_3, x_3) = -\frac{e^{-|\xi||y_3-x_3|}}{4\pi|\xi|} + \left(\frac{Z_\varepsilon + |\xi|}{Z_\varepsilon - |\xi|}\right)\frac{e^{-|\xi|(y_3+x_3)}}{4\pi|\xi|}. \tag{4.37}$$

c) Analysis of singularities

To obtain the spectral Green's function $\widehat{G}$ without dissipation, the limit $\varepsilon \to 0$ has to be taken in (4.37). This can be done directly wherever the limit is regular and continuous on ξ. Singular points, on the other hand, have to be analyzed carefully to fulfill correctly the limiting absorption principle. Thus we study first the singularities of the limit function before applying this principle, i.e., considering just $\varepsilon = 0$, in which case we have

$$\widehat{G}_0(\xi) = -\frac{e^{-|\xi||y_3-x_3|}}{4\pi|\xi|} + \left(\frac{Z_\infty + |\xi|}{Z_\infty - |\xi|}\right)\frac{e^{-|\xi|(y_3+x_3)}}{4\pi|\xi|}. \tag{4.38}$$

Possible singularities for (4.38) may only appear when $|\xi| = 0$ or when $|\xi| = Z_\infty$, i.e., when the denominator of the fractions is zero. Otherwise the function is regular and continuous.

For $|\xi| = 0$ the function (4.38) is continuous. This can be seen by writing it, analogously as in Durán, Muga & Nédélec (2005*b*), in the form

$$\widehat{G}_0(\xi) = \frac{H\big(|\xi|\big)}{|\xi|}, \tag{4.39}$$

where

$$H(\beta) = \frac{1}{4\pi}\left(-e^{-\beta\,|y_3-x_3|} + \frac{Z_\infty + \beta}{Z_\infty - \beta}\,e^{-\beta\,(y_3+x_3)}\right), \qquad \beta \in \mathbb{C}. \tag{4.40}$$

Since $H(\beta)$ is an analytic function in $\beta = 0$, since $H(0) = 0$, and since

$$\lim_{|\xi|\to 0} \widehat{G}_0(\xi) = \lim_{|\xi|\to 0} \frac{H\big(|\xi|\big) - H(0)}{|\xi|} = H'(0), \tag{4.41}$$

we can easily obtain that

$$\lim_{|\xi|\to 0} \widehat{G}_0(\xi) = \frac{1}{4\pi}\left(1 + \frac{1}{Z_\infty} + |y_3 - x_3| - (y_3 + x_3)\right), \tag{4.42}$$

being thus $\widehat{G}_0$ bounded and continuous on $|\xi| = 0$.

For $\xi = Z_\infty$ and $\xi = -Z_\infty$, the function (4.38) presents two simple poles, whose residues are characterized by

$$\lim_{\xi\to\pm Z_\infty} (\xi \mp Z_\infty)\widehat{G}_0(\xi) = \mp\frac{1}{2\pi}\,e^{-Z_\infty(y_3+x_3)}. \tag{4.43}$$

To analyze the effect of this singularity, we study now the computation of the inverse Fourier transform of

$$\widehat{G}_P(\xi) = \frac{1}{2\pi}\,e^{-Z_\infty(y_3+x_3)}\left(\frac{1}{\xi + Z_\infty} - \frac{1}{\xi - Z_\infty}\right), \tag{4.44}$$

which has to be done in the frame of the limiting absorption principle to obtain the correct physical results, i.e., the inverse Fourier transform has to be understood in the sense of

$$G_P(\boldsymbol{x},\boldsymbol{y}) = \lim_{\varepsilon\to 0}\left\{\frac{e^{-Z_\varepsilon(y_3+x_3)}}{4\pi^2}\int_0^\pi\int_{-\infty}^{\infty}\left(\frac{1}{\xi+Z_\varepsilon}-\frac{1}{\xi-Z_\varepsilon}\right)|\xi|\,e^{i\xi r\sin\theta\cos(\psi-\varphi)}\,\mathrm{d}\xi\,\mathrm{d}\psi\right\}, \tag{4.45}$$

being the spatial variables inside the integrals expressed through the spherical coordinates

$$\begin{cases} y_1-x_1 = r\sin\theta\cos\varphi, \\ y_2-x_2 = r\sin\theta\sin\varphi, \\ y_3-x_3 = r\cos\theta, \end{cases} \quad \text{for} \quad \begin{cases} 0\le r<\infty, \\ 0\le\theta\le\pi, \\ -\pi<\varphi\le\pi. \end{cases} \tag{4.46}$$

To perform correctly the computation of (4.45), we apply the residue theorem of complex analysis (cf., e.g., Arfken & Weber 2005, Bak & Newman 1997, Dettman 1984) on the complex meromorphic mapping

$$F(\xi) = \left(\frac{1}{\xi+\xi_p}-\frac{1}{\xi-\xi_p}\right)|\xi|\,e^{i\xi\tau}, \tag{4.47}$$

which admits two simple poles at ξ_p and $-\xi_p$, where $\mathfrak{Im}\{\xi_p\}>0$ and $\tau\in\mathbb{R}$. We consider also the closed complex integration contours $C^+_{R,\varepsilon}$ and $C^-_{R,\varepsilon}$, which are associated respectively with the values $\tau\ge 0$ and $\tau<0$, and are depicted in Figure 4.3.

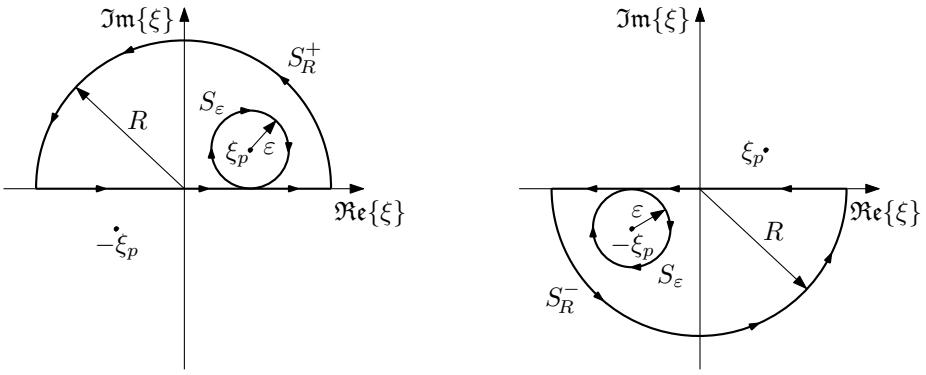

(a) Contour $C^+_{R,\varepsilon}$ (b) Contour $C^-_{R,\varepsilon}$

FIGURE 4.3. Complex integration contours using the limiting absorption principle.

Since the contours $C^+_{R,\varepsilon}$ and $C^-_{R,\varepsilon}$ enclose no singularities, the residue theorem of Cauchy implies that the respective closed path integrals are zero, i.e.,

$$\oint_{C^+_{R,\varepsilon}} F(\xi)\,\mathrm{d}\xi = 0, \tag{4.48}$$

and

$$\oint_{C^-_{R,\varepsilon}} F(\xi)\,\mathrm{d}\xi = 0. \tag{4.49}$$

By considering $\tau \geq 0$ and working with the contour $C^+_{R,\varepsilon}$ in the upper complex plane, we obtain from (4.48) that

$$\int_{-R}^{\mathfrak{Re}\{\xi_p\}} F(\xi)\,\mathrm{d}\xi + \int_{S_\varepsilon} F(\xi)\,\mathrm{d}\xi + \int_{\mathfrak{Re}\{\xi_p\}}^{R} F(\xi)\,\mathrm{d}\xi + \int_{S_R^+} F(\xi)\,\mathrm{d}\xi = 0. \tag{4.50}$$

Performing the change of variable $\xi - \xi_p = \varepsilon e^{i\phi}$ for the integral on S_ε yields

$$\int_{S_\varepsilon} F(\xi)\,\mathrm{d}\xi = i\,e^{i\xi_p\tau} \int_{3\pi/2}^{-\pi/2} \left(\frac{\varepsilon e^{i\phi}}{\varepsilon e^{i\phi} + 2\xi_p} - 1 \right) |\xi_p + \varepsilon e^{i\phi}|\, e^{\varepsilon\tau(i\cos\phi - \sin\phi)}\,\mathrm{d}\phi. \tag{4.51}$$

By taking then the limit $\varepsilon \to 0$ we obtain

$$\lim_{\varepsilon\to 0} \int_{S_\varepsilon} F(\xi)\,\mathrm{d}\xi = i2\pi|\xi_p|e^{i\xi_p\tau}. \tag{4.52}$$

In a similar way, taking $\xi = Re^{i\phi}$ for the integral on S_R^+ yields

$$\int_{S_R^+} F(\xi)\,\mathrm{d}\xi = \int_0^\pi \left(\frac{iR^2 e^{i\phi}}{Re^{i\phi} + \xi_p} - \frac{iR^2 e^{i\phi}}{Re^{i\phi} - \xi_p} \right) e^{R\tau(i\cos\phi - \sin\phi)}\,\mathrm{d}\phi. \tag{4.53}$$

Since $|e^{iR\tau\cos\phi}| \leq 1$ and $R\sin\phi \geq 0$ for $0 \leq \phi \leq \pi$, when taking the limit $R \to \infty$ we obtain

$$\lim_{R\to\infty} \int_{S_R^+} F(\xi)\,\mathrm{d}\xi = 0. \tag{4.54}$$

Thus, taking the limits $\varepsilon \to 0$ and $R \to \infty$ in (4.50) yields

$$\int_{-\infty}^{\infty} F(\xi)\,\mathrm{d}\xi = -i2\pi|\xi_p|e^{i\xi_p\tau}, \qquad \tau \geq 0. \tag{4.55}$$

By considering now $\tau < 0$ and working with the contour $C^-_{R,\varepsilon}$ in the lower complex plane, we obtain from (4.49) that

$$\int_{R}^{\mathfrak{Re}\{-\xi_p\}} F(\xi)\,\mathrm{d}\xi + \int_{S_\varepsilon} F(\xi)\,\mathrm{d}\xi + \int_{\mathfrak{Re}\{-\xi_p\}}^{-R} F(\xi)\,\mathrm{d}\xi + \int_{S_R^-} F(\xi)\,\mathrm{d}\xi = 0. \tag{4.56}$$

Performing the change of variable $\xi + \xi_p = \varepsilon e^{i\phi}$ for the integral on S_ε yields

$$\int_{S_\varepsilon} F(\xi)\,\mathrm{d}\xi = i\,e^{-i\xi_p\tau} \int_{\pi/2}^{-3\pi/2} \left(1 - \frac{\varepsilon e^{i\phi}}{\varepsilon e^{i\phi} - 2\xi_p} \right) |\xi_p - \varepsilon e^{i\phi}|\, e^{\varepsilon\tau(i\cos\phi - \sin\phi)}\,\mathrm{d}\phi. \tag{4.57}$$

By taking then the limit $\varepsilon \to 0$ we obtain

$$\lim_{\varepsilon\to 0} \int_{S_\varepsilon} F(\xi)\,\mathrm{d}\xi = -i2\pi|\xi_p|e^{-i\xi_p\tau}. \tag{4.58}$$

In a similar way, taking $\xi = Re^{i\phi}$ for the integral on S_R^- yields

$$\int_{S_R^-} F(\xi)\,\mathrm{d}\xi = \int_{-\pi}^0 \left(\frac{iR^2 e^{i\phi}}{Re^{i\phi} + \xi_p} - \frac{iR^2 e^{i\phi}}{Re^{i\phi} - \xi_p} \right) e^{R\tau(i\cos\phi - \sin\phi)}\,\mathrm{d}\phi. \tag{4.59}$$

Since $|e^{iR\tau\cos\phi}| \leq 1$ and $R\sin\phi \leq 0$ for $-\pi \leq \phi \leq 0$, when taking the limit $R \to \infty$ we obtain

$$\lim_{R\to\infty} \int_{S_R^-} F(\xi)\,\mathrm{d}\xi = 0. \tag{4.60}$$

Thus, taking the limits $\varepsilon \to 0$ and $R \to \infty$ in (4.56) yields

$$\int_{-\infty}^{\infty} F(\xi)\,\mathrm{d}\xi = -i2\pi|\xi_p|e^{-i\xi_p\tau}, \qquad \tau < 0. \tag{4.61}$$

In conclusion, from (4.55) and (4.61) we obtain that

$$\int_{-\infty}^{\infty} F(\xi)\,\mathrm{d}\xi = -i2\pi|\xi_p|e^{i\xi_p|\tau|}, \qquad \tau \in \mathbb{R}. \tag{4.62}$$

Using (4.62) for $\xi_p = Z_\infty$ and $\tau = r\sin\theta\cos(\psi-\varphi)$ yields then that the inverse Fourier transform of (4.44), when considering the limiting absorption principle, is given by

$$G_P^L(\boldsymbol{x},\boldsymbol{y}) = -\frac{iZ_\infty}{2\pi}\,e^{-Z_\infty(y_3+x_3)}\int_0^\pi e^{iZ_\infty r\sin\theta\,|\cos(\psi-\varphi)|}\,\mathrm{d}\psi. \tag{4.63}$$

It can be observed that the integral in (4.63) is independent of the angle φ, which we can choose without problems as $\varphi = \pi/2$ and therefore $|\cos(\psi-\varphi)| = \sin\psi$. Since

$$r\sin\theta = |\boldsymbol{y}_s - \boldsymbol{x}_s|, \tag{4.64}$$

we can express (4.63) as

$$G_P^L(\boldsymbol{x},\boldsymbol{y}) = -\frac{iZ_\infty}{2\pi}\,e^{-Z_\infty(y_3+x_3)}\int_0^\pi e^{iZ_\infty|\boldsymbol{y}_s-\boldsymbol{x}_s|\sin\psi}\,\mathrm{d}\psi. \tag{4.65}$$

We observe that this expression describes the asymptotic behavior of the surface waves, which are linked to the presence of the poles in the spectral Green's function. Due (A.112) and (A.244), we can rewrite (4.65) more explicitly as

$$G_P^L(\boldsymbol{x},\boldsymbol{y}) = -\frac{iZ_\infty}{2}\,e^{-Z_\infty(y_3+x_3)}\Big[J_0\big(Z_\infty|\boldsymbol{y}_s-\boldsymbol{x}_s|\big) + i\boldsymbol{H}_0\big(Z_\infty|\boldsymbol{y}_s-\boldsymbol{x}_s|\big)\Big], \tag{4.66}$$

where J_0 denotes the Bessel function of order zero (vid. Subsection A.2.4) and $\boldsymbol{H}_0$ the Struve function of order zero (vid. Subsection A.2.7).

If the limiting absorption principle is not considered, i.e., if $\mathfrak{Im}\{\xi_p\} = 0$, then the inverse Fourier transform of (4.44) could be computed in the sense of the principal value with the residue theorem by considering, instead of $C_{R,\varepsilon}^+$ and $C_{R,\varepsilon}^-$, the contours depicted in Figure 4.4. In this case we would obtain, instead of (4.62), the quantity

$$\int_{-\infty}^{\infty} F(\xi)\,\mathrm{d}\xi = 2\pi|\xi_p|\sin\big(\xi_p|\tau|\big), \qquad \tau \in \mathbb{R}. \tag{4.67}$$

The inverse Fourier transform of (4.44) would be in this case

$$G_P^{NL}(\boldsymbol{x},\boldsymbol{y}) = \frac{Z_\infty}{2}\,e^{-Z_\infty(y_3+x_3)}\boldsymbol{H}_0\big(Z_\infty|\boldsymbol{y}_s-\boldsymbol{x}_s|\big), \tag{4.68}$$

which is correct from the mathematical point of view, but yields only a standing surface wave, and not a desired outgoing progressive surface wave as in (4.66).

The effect of the limiting absorption principle, in the spatial dimension, is then given by the difference between (4.66) and (4.68), i.e., by

$$G_L(\boldsymbol{x},\boldsymbol{y}) = G_P^L(\boldsymbol{x},\boldsymbol{y}) - G_P^{NL}(\boldsymbol{x},\boldsymbol{y}) = -\frac{iZ_\infty}{2}\,e^{-Z_\infty(y_3+x_3)}J_0\big(Z_\infty|\boldsymbol{y}_s-\boldsymbol{x}_s|\big), \tag{4.69}$$

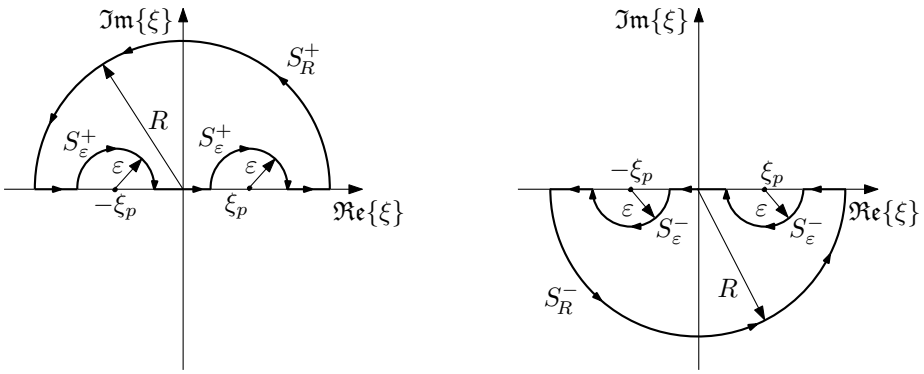

(a) Contour $C_{R,\varepsilon}^+$ (b) Contour $C_{R,\varepsilon}^-$

FIGURE 4.4. Complex integration contours without using the limiting absorption principle.

whose Fourier transform, and therefore the spectral effect, is given by

$$\widehat{G}_L(\xi) = \widehat{G}_P^L(\xi) - \widehat{G}_P^{NL}(\xi) = -\frac{iZ_\infty}{2|\xi|}\, e^{-Z_\infty(y_3+x_3)}\big[\delta(\xi - Z_\infty) + \delta(\xi + Z_\infty)\big]. \tag{4.70}$$

d) Spectral Green's function without dissipation

The spectral Green's function $\widehat{G}$ without dissipation is therefore obtained by taking the limit $\varepsilon \to 0$ in (4.37) and considering the effect of the limiting absorption principle for the appearing singularities, summarized in (4.70). Thus we obtain in the sense of distributions

$$\begin{aligned}\widehat{G}(\xi; y_3, x_3) = &- \frac{e^{-|\xi||y_3 - x_3|}}{4\pi|\xi|} + \left(\frac{Z_\infty + |\xi|}{Z_\infty - |\xi|}\right)\frac{e^{-|\xi|(y_3+x_3)}}{4\pi|\xi|} \\ &- \frac{iZ_\infty}{2|\xi|}\, e^{-Z_\infty(y_3+x_3)}\big[\delta(\xi - Z_\infty) + \delta(\xi + Z_\infty)\big].\end{aligned} \tag{4.71}$$

For our further analysis, this spectral Green's function is decomposed into four terms according to

$$\widehat{G} = \widehat{G}_\infty + \widehat{G}_N + \widehat{G}_L + \widehat{G}_R, \tag{4.72}$$

where

$$\widehat{G}_\infty(\xi; y_3, x_3) = -\frac{e^{-|\xi||y_3 - x_3|}}{4\pi|\xi|}, \tag{4.73}$$

$$\widehat{G}_N(\xi; y_3, x_3) = -\frac{e^{-|\xi|(y_3+x_3)}}{4\pi|\xi|}, \tag{4.74}$$

$$\widehat{G}_L(\xi; y_3, x_3) = -\frac{iZ_\infty}{2|\xi|}\, e^{-Z_\infty(y_3+x_3)}\big[\delta(\xi - Z_\infty) + \delta(\xi + Z_\infty)\big], \tag{4.75}$$

$$\widehat{G}_R(\xi; y_3, x_3) = \frac{Z_\infty e^{-|\xi|(y_3+x_3)}}{2\pi|\xi|\big(Z_\infty - |\xi|\big)}. \tag{4.76}$$

4.3.4 Spatial Green's function

a) Spatial Green's function as an inverse Fourier transform

The desired spatial Green's function is then given by the inverse Fourier transform of the spectral Green's function (4.71), namely by

$$\begin{aligned} G(\boldsymbol{x},\boldsymbol{y}) = &- \frac{1}{8\pi^2}\int_{-\infty}^{\infty}\int_{0}^{\pi} e^{-|\xi||y_3-x_3|}\, e^{i\xi r\sin\theta\cos(\psi-\varphi)}\,\mathrm{d}\psi\,\mathrm{d}\xi \\ &+ \frac{1}{8\pi^2}\int_{-\infty}^{\infty}\int_{0}^{\pi} \left(\frac{Z_\infty+|\xi|}{Z_\infty-|\xi|}\right) e^{-|\xi|(y_3+x_3)}\, e^{i\xi r\sin\theta\cos(\psi-\varphi)}\,\mathrm{d}\psi\,\mathrm{d}\xi \\ &- \frac{iZ_\infty}{2}\, e^{-Z_\infty(y_3+x_3)} J_0\big(Z_\infty|\boldsymbol{y}_s-\boldsymbol{x}_s|\big), \end{aligned} \tag{4.77}$$

where the spherical coordinates (4.46) are used again inside the integrals.

Due the linearity of the Fourier transform, the decomposition (4.72) applies also in the spatial domain, i.e., the spatial Green's function is decomposed in the same manner by

$$G = G_\infty + G_N + G_L + G_R. \tag{4.78}$$

b) Term of the full-space Green's function

The first term in (4.77) corresponds to the inverse Fourier transform of (4.73), and can be rewritten, due (A.794), as the Hankel transform

$$G_\infty(\boldsymbol{x},\boldsymbol{y}) = -\frac{1}{4\pi}\int_0^\infty e^{-\rho|y_3-x_3|} J_0\big(\rho|\boldsymbol{y}_s-\boldsymbol{x}_s|\big)\,\mathrm{d}\rho. \tag{4.79}$$

The value for this integral can be obtained either from Watson (1944, page 384), by using Sommerfeld's formula (Magnus & Oberhettinger 1954, page 34) for $k=0$, i.e.,

$$\int_0^\infty e^{-\rho|y_3-x_3|} J_0\big(\rho|\boldsymbol{y}_s-\boldsymbol{x}_s|\big)\,\mathrm{d}\rho = \frac{1}{|\boldsymbol{y}-\boldsymbol{x}|}, \tag{4.80}$$

from Gradshteyn & Ryzhik (2007, equation 6.611–1), or by directly computing the two integrals appearing in the first term of (4.77), beginning with the exterior one. This way, the inverse Fourier transform of (4.73) is readily given by

$$G_\infty(\boldsymbol{x},\boldsymbol{y}) = -\frac{1}{4\pi|\boldsymbol{y}-\boldsymbol{x}|}. \tag{4.81}$$

We observe that (4.81) is, in fact, the full-space Green's function of the Laplace equation. Thus $G_N+G_L+G_R$ represents the perturbation of the full-space Green's function G_∞ due the presence of the impedance half-space.

c) Term associated with a Neumann boundary condition

The inverse Fourier transform of (4.74) is computed in the same manner as the term G_∞. It is given by

$$G_N(\boldsymbol{x},\boldsymbol{y}) = -\frac{1}{4\pi}\int_0^\infty e^{-\rho(y_3+x_3)} J_0\big(\rho|\boldsymbol{y}_s-\boldsymbol{x}_s|\big)\,\mathrm{d}\rho, \tag{4.82}$$

and in this case, instead of (4.80), Sommerfeld's formula becomes

$$\int_0^\infty e^{-\rho(y_3+x_3)} J_0\big(\rho|\boldsymbol{y}_s - \boldsymbol{x}_s|\big)\,\mathrm{d}\rho = \frac{1}{|\boldsymbol{y} - \bar{\boldsymbol{x}}|}, \tag{4.83}$$

where $\bar{\boldsymbol{x}} = (x_1, x_2, -x_3)$ corresponds to the image point of $\boldsymbol{x}$ in the lower half-space. The inverse Fourier transform of (4.74) is therefore given by

$$G_N(\boldsymbol{x}, \boldsymbol{y}) = -\frac{1}{4\pi|\boldsymbol{y} - \bar{\boldsymbol{x}}|}, \tag{4.84}$$

which represents the additional term that appears in the Green's function due the method of images when considering a Neumann boundary condition, as in (4.21).

d) Term associated with the limiting absorption principle

The term G_L, the inverse Fourier transform of (4.75), is associated with the effect of the limiting absorption principle on the Green's function, and has been already calculated in (4.69). It yields the imaginary part of the Green's function, and is given by

$$G_L(\boldsymbol{x}, \boldsymbol{y}) = -\frac{iZ_\infty}{2}\, e^{-Z_\infty(y_3+x_3)} J_0\big(Z_\infty|\boldsymbol{y}_s - \boldsymbol{x}_s|\big). \tag{4.85}$$

e) Remaining term

The remaining term G_R, the inverse Fourier transform of (4.76), can be computed as the integral

$$G_R(\boldsymbol{x}, \boldsymbol{y}) = \frac{Z_\infty}{2\pi} \int_0^\infty \frac{e^{-\rho(y_3+x_3)}}{Z_\infty - \rho} J_0\big(\rho|\boldsymbol{y}_s - \boldsymbol{x}_s|\big)\,\mathrm{d}\rho. \tag{4.86}$$

We denote

$$\varrho_s = |\boldsymbol{y}_s - \boldsymbol{x}_s| \qquad \text{and} \qquad v_3 = y_3 + x_3, \tag{4.87}$$

and we consider the change of notation

$$G_R(\boldsymbol{x}, \boldsymbol{y}) = \frac{Z_\infty}{2\pi}\, e^{-Z_\infty v_3} G_B(\varrho_s, v_3), \tag{4.88}$$

being

$$G_B(\varrho_s, v_3) = \int_0^\infty \frac{e^{(Z_\infty-\rho)v_3}}{Z_\infty - \rho} J_0(\varrho_s\rho)\,\mathrm{d}\rho. \tag{4.89}$$

Consequently, by considering (4.83) we have for the y_3-derivative of G_B that

$$\frac{\partial G_B}{\partial y_3}(\varrho_s, v_3) = e^{Z_\infty v_3} \int_0^\infty e^{-\rho v_3} J_0(\varrho_s\rho)\,\mathrm{d}\rho = \frac{e^{Z_\infty v_3}}{|\boldsymbol{y} - \bar{\boldsymbol{x}}|}. \tag{4.90}$$

Following Pidcock (1985), the integral (4.86) can be thus expressed by

$$G_R(\boldsymbol{x}, \boldsymbol{y}) = \frac{Z_\infty}{2\pi}\, e^{-Z_\infty v_3} \left(G_B(\varrho_s, 0) + \int_0^{v_3} \frac{e^{Z_\infty \eta}}{\sqrt{\varrho_s^2 + \eta^2}}\,\mathrm{d}\eta \right), \tag{4.91}$$

where

$$G_B(\varrho_s, 0) = \int_0^\infty \frac{J_0(\varrho_s\rho)}{Z_\infty - \rho}\,\mathrm{d}\rho. \tag{4.92}$$

To evaluate the integral (4.92), we consider the closed complex integration contour $C_{R,\varepsilon}$ depicted in Figure 4.5 and use the fact that

$$\oint_{C_{R,\varepsilon}} \frac{H_0^{(1)}(\varrho_s \rho)}{Z_\infty - \rho} \, \mathrm{d}\rho = 0, \tag{4.93}$$

where $H_0^{(1)}$ denotes the zeroth order Hankel function of the first kind (vid. Subsection A.2.4).

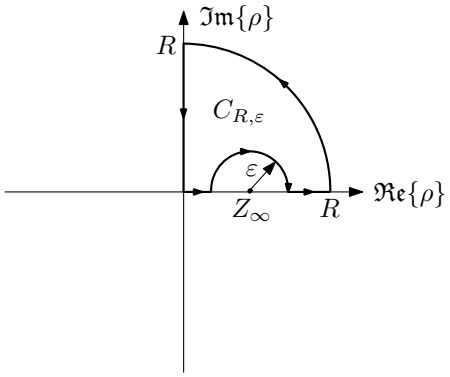

FIGURE 4.5. Complex integration contour $C_{R,\varepsilon}$.

We can express (4.93) more explicitly as

$$\begin{aligned} &\int_0^{Z_\infty - \varepsilon} \frac{H_0^{(1)}(\varrho_s \rho)}{Z_\infty - \rho} \, \mathrm{d}\rho - i \int_\pi^0 H_0^{(1)}\Big(\varrho_s\big(Z_\infty + \varepsilon e^{i\theta}\big)\Big) \, \mathrm{d}\theta + \int_{Z_\infty + \varepsilon}^R \frac{H_0^{(1)}(\varrho_s \rho)}{Z_\infty - \rho} \, \mathrm{d}\rho \\ &\quad - i \int_0^{\pi/2} \frac{H_0^{(1)}\big(\varrho_s R e^{i\theta}\big)}{Z_\infty - R e^{i\theta}} \, R e^{i\theta} \, \mathrm{d}\theta - \frac{2}{\pi} \int_0^R \frac{K_0(\varrho_s \tau)}{Z_\infty - i\tau} \, \mathrm{d}\tau = 0, \end{aligned} \tag{4.94}$$

where we use the relation (A.153) for $\nu = 0$ and where K_0 denotes the zeroth order modified Bessel function of the second kind (vid. Subsection A.2.5). By taking the limits $\varepsilon \to 0$ and $R \to \infty$ we obtain that

$$\int_0^\infty \frac{H_0^{(1)}(\varrho_s \rho)}{Z_\infty - \rho} \, \mathrm{d}\rho + i\pi H_0^{(1)}(Z_\infty \varrho_s) - \frac{2}{\pi} \int_0^\infty \left(\frac{Z_\infty + i\tau}{Z_\infty^2 + \tau^2} \right) K_0(\varrho_s \tau) \, \mathrm{d}\tau = 0, \tag{4.95}$$

where the integral on R tends to zero due the asymptotic behavior (A.139) of the Hankel function $H_0^{(1)}$. Considering the real part in (4.95) and rearranging yields

$$\int_0^\infty \frac{J_0(\varrho_s \rho)}{Z_\infty - \rho} \, \mathrm{d}\rho = \pi Y_0(Z_\infty \varrho_s) + \frac{2 Z_\infty}{\pi} \int_0^\infty \frac{K_0(\varrho_s \tau)}{Z_\infty^2 + \tau^2} \, \mathrm{d}\tau, \tag{4.96}$$

where Y_0 denotes the Neumann function of order zero. The integral on the right-hand side of (4.96) is given by (Gradshteyn & Ryzhik 2007, equation 6.566–4)

$$\frac{2 Z_\infty}{\pi} \int_0^\infty \frac{K_0(\varrho_s \tau)}{Z_\infty^2 + \tau^2} \, \mathrm{d}\tau = \frac{\pi}{2} \big[\boldsymbol{H}_0(Z_\infty \varrho_s) - Y_0(Z_\infty \varrho_s) \big]. \tag{4.97}$$

Hence, from (4.96) and (4.97) we get that

$$G_B(\varrho_s, 0) = \frac{\pi}{2} \big[\boldsymbol{H}_0(Z_\infty \varrho_s) + Y_0(Z_\infty \varrho_s) \big]. \tag{4.98}$$

By replacing in (4.91), we can express the remaining term G_R as

$$G_R(\boldsymbol{x},\boldsymbol{y}) = \frac{Z_\infty}{4}\, e^{-Z_\infty v_3}\left(Y_0(Z_\infty \varrho_s) + \boldsymbol{H}_0(Z_\infty \varrho_s) + \frac{2}{\pi}\int_0^{v_3} \frac{e^{Z_\infty \eta}}{\sqrt{\varrho_s^2+\eta^2}}\,\mathrm{d}\eta\right), \tag{4.99}$$

which corresponds to the representation derived by Kim (1965) and which was implicit in the work of Havelock (1955). For the remaining integral in (4.99), we consider the fact that

$$\int_0^{v_3} \frac{e^{Z_\infty \eta}}{\sqrt{\varrho_s^2+\eta^2}}\,\mathrm{d}\eta = \int_0^{Z_\infty v_3} \frac{e^{\alpha}}{\sqrt{Z_\infty^2\varrho_s^2+\alpha^2}}\,\mathrm{d}\alpha, \tag{4.100}$$

where we appreciate that the impedance Z_∞ appears only as a scaling factor for the variables ϱ_s and v_3. We can hence simplify the notation, by assuming temporarily that $Z_\infty = 1$ and by scaling the result at the end correspondingly by Z_∞. The power series expansion (A.8) of the exponential function implies that

$$\int_0^{v_3} \frac{e^{\eta}}{\sqrt{\varrho_s^2+\eta^2}}\,\mathrm{d}\eta = \sum_{n=0}^{\infty}\int_0^{v_3} \frac{\eta^n}{n!\sqrt{\varrho_s^2+\eta^2}}\,\mathrm{d}\eta. \tag{4.101}$$

Let us denote

$$I_n = \int_0^{v_3} \frac{\eta^n}{n!\sqrt{\varrho_s^2+\eta^2}}\,\mathrm{d}\eta, \tag{4.102}$$

in which case we can show by mathematical induction and by computing carefully (using, e.g., Gradshteyn & Ryzhik 2007, Dwight 1957, or Prudnikov et al. 1992) that

$$I_0 = \ln\Bigl(v_3 + \sqrt{\varrho_s^2+v_3^2}\Bigr), \tag{4.103}$$

$$I_1 = \sqrt{\varrho_s^2+v_3^2}\,, \tag{4.104}$$

$$\begin{aligned} I_{2n} = {}& \sqrt{\varrho_s^2+v_3^2}\,\sum_{m=0}^{n-1}(-1)^m \frac{2^{2n-2m-2}\bigl((n-m-1)!\bigr)^2}{(2n-2m-1)!\,2^{2n}(n!)^2}\, v_3^{2n-2m-1}\varrho_s^{2m} \\ & + \frac{(-1)^n}{(n!)^2}\left(\frac{\varrho_s}{2}\right)^{2n}\left(\ln\Bigl(v_3+\sqrt{\varrho_s^2+v_3^2}\Bigr) - \ln(\varrho_s)\right) \qquad (n=1,2,\ldots), \end{aligned} \tag{4.105}$$

$$\begin{aligned} I_{2n+1} = {}& \sqrt{\varrho_s^2+v_3^2}\,\sum_{m=0}^{n}(-1)^m \frac{(2n-2m)!}{2^{2n-2m}\bigl((n-m)!\bigr)^2}\left(\frac{2^n\,n!}{(2n+1)!}\right)^2 v_3^{2n-2m}\varrho_s^{2m} \\ & - (-1)^n \frac{2^{2n}(n!)^2}{\bigl((2n+1)!\bigr)^2}\,\varrho_s^{2n+1} \qquad (n=1,2,\ldots). \end{aligned} \tag{4.106}$$

We remark that (4.106) can be equivalently expressed as

$$\begin{aligned} I_{2n+1} = {}& \frac{1}{(2n+1)!}\sum_{m=0}^{n}\frac{n!}{m!\,(n-m)!}\,(-1)^m\varrho_s^{2m}\frac{\left(\sqrt{\varrho_s^2+v_3^2}\right)^{2n-2m+1}}{2n-2m+1} \\ & - (-1)^n \frac{2^{2n}(n!)^2}{\bigl((2n+1)!\bigr)^2}\,\varrho_s^{2n+1} \qquad (n=1,2,\ldots). \end{aligned} \tag{4.107}$$

We observe that the second term in (4.105) is linked with the series expansion (A.99) of the Bessel function J_0, whereas the second term in (4.106) and (4.107) is associated with

the series expansion (A.239) of the Struve function $\boldsymbol{H}_0$. Replacing these values in the right-hand side of (4.101) and rearranging yields

$$\int_0^{v_3} \frac{e^{\eta}}{\sqrt{\varrho_s^2+\eta^2}}\,\mathrm{d}\eta = J_0(\varrho_s)\Big(\ln\Big(v_3+\sqrt{\varrho_s^2+v_3^2}\Big)-\ln(\varrho_s)\Big)-\frac{\pi}{2}\boldsymbol{H}_0(\varrho_s) + \sqrt{\varrho_s^2+v_3^2}\,\Big(\mathrm{So}(\varrho_s,v_3)+\mathrm{Se}(\varrho_s,v_3)\Big), \tag{4.108}$$

where

$$\mathrm{So}(\varrho_s,v_3)=\sum_{n=0}^{\infty}\sum_{m=0}^{\infty}(-1)^m\frac{2^{2n}(n!)^2\,v_3^{2n+1}\varrho_s^{2m}}{(2n+1)!\,2^{2(m+n+1)}\big((m+n+1)!\big)^2}, \tag{4.109}$$

$$\mathrm{Se}(\varrho_s,v_3)=\sum_{n=0}^{\infty}\sum_{m=0}^{\infty}(-1)^m\frac{(2n)!}{2^{2n}(n!)^2}\left(\frac{2^{m+n}(m+n)!}{(2n+2m+1)!}\right)^2 v_3^{2n}\varrho_s^{2m}. \tag{4.110}$$

Due (4.107), we could express (4.110) alternatively as

$$\mathrm{Se}(\varrho_s,v_3)=\sum_{n=0}^{\infty}\frac{1}{(2n+1)!}\sum_{m=0}^{n}\frac{n!}{m!\,(n-m)!}\big(-\varrho_s^2\big)^m\frac{\Big(\sqrt{\varrho_s^2+v_3^2}\Big)^{2n-2m}}{2n-2m+1}. \tag{4.111}$$

Similar series expansions can be found in the article of Noblesse (1982). Scaling again the variables ϱ_s and v_3 by Z_∞ in (4.108) and replacing in (4.99) implies that

$$\begin{aligned}G_R(\boldsymbol{x},\boldsymbol{y}) = {}& \frac{Z_\infty}{2\pi}\,e^{-Z_\infty v_3}J_0(Z_\infty\varrho_s)\ln\Big(Z_\infty v_3+Z_\infty\sqrt{\varrho_s^2+v_3^2}\Big)\\ &+\frac{Z_\infty}{4}\,e^{-Z_\infty v_3}\left(Y_0(Z_\infty\varrho_s)-\frac{2}{\pi}J_0(Z_\infty\varrho_s)\ln(Z_\infty\varrho_s)\right)\\ &+\frac{Z_\infty^2}{2\pi}\sqrt{\varrho_s^2+v_3^2}\;e^{-Z_\infty v_3}\Big(\mathrm{So}\big(Z_\infty\varrho_s,Z_\infty v_3\big)+\mathrm{Se}\big(Z_\infty\varrho_s,Z_\infty v_3\big)\Big).\end{aligned} \tag{4.112}$$

f) Complete spatial Green's function

The desired complete spatial Green's function is finally obtained, as stated in (4.78), by adding the terms (4.81), (4.84), (4.85), and (4.112). It is depicted graphically for $Z_\infty=1$ and $\boldsymbol{x}=(0,0,2)$ in Figures 4.6 & 4.7, and given explicitly by

$$\begin{aligned}G(\boldsymbol{x},\boldsymbol{y}) = {}& -\frac{1}{4\pi|\boldsymbol{y}-\boldsymbol{x}|}-\frac{1}{4\pi|\boldsymbol{y}-\bar{\boldsymbol{x}}|}-\frac{iZ_\infty}{2}\,e^{-Z_\infty v_3}J_0(Z_\infty\varrho_s)\\ &+\frac{Z_\infty}{2\pi}\,e^{-Z_\infty v_3}J_0(Z_\infty\varrho_s)\ln\Big(Z_\infty v_3+Z_\infty\sqrt{\varrho_s^2+v_3^2}\Big)\\ &+\frac{Z_\infty}{4}\,e^{-Z_\infty v_3}\left(Y_0(Z_\infty\varrho_s)-\frac{2}{\pi}J_0(Z_\infty\varrho_s)\ln(Z_\infty\varrho_s)\right)\\ &+\frac{Z_\infty^2}{2\pi}\sqrt{\varrho_s^2+v_3^2}\;e^{-Z_\infty v_3}\Big(\mathrm{So}\big(Z_\infty\varrho_s,Z_\infty v_3\big)+\mathrm{Se}\big(Z_\infty\varrho_s,Z_\infty v_3\big)\Big),\end{aligned} \tag{4.113}$$

where the notation (4.87) is used and where the functions So and Se are defined respectively in (4.109) and (4.110).

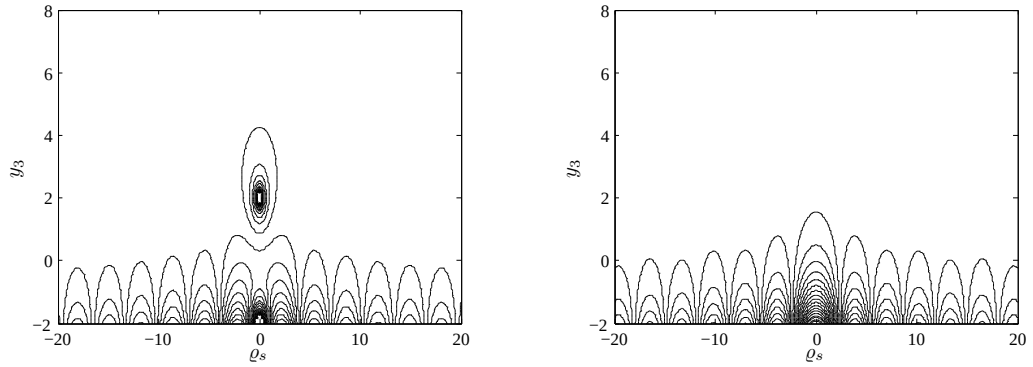

(a) Real part (b) Imaginary part

FIGURE 4.6. Contour plot of the complete spatial Green's function.

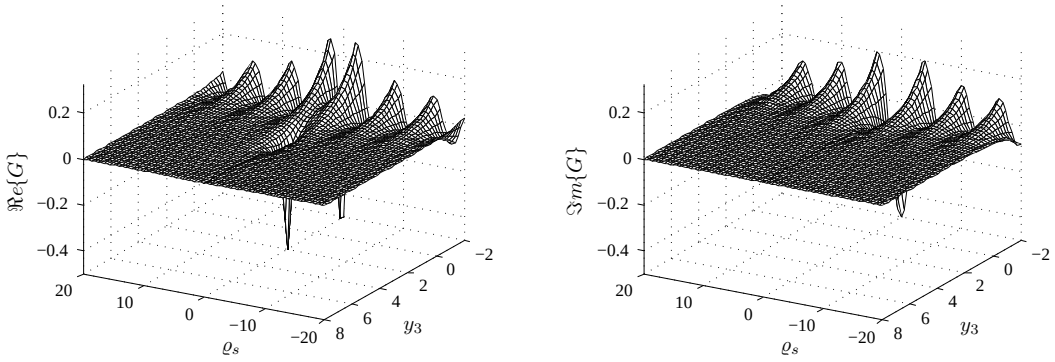

(a) Real part (b) Imaginary part

FIGURE 4.7. Oblique view of the complete spatial Green's function.

For the derivative of the Green's function with respect to the y_3-variable, it holds that

$$\frac{\partial G}{\partial y_3}(\boldsymbol{x},\boldsymbol{y}) = \frac{y_3 - x_3}{4\pi|\boldsymbol{y}-\boldsymbol{x}|^3} + \frac{v_3}{4\pi|\boldsymbol{y}-\bar{\boldsymbol{x}}|^3} + \frac{iZ_\infty^2}{2}\, e^{-Z_\infty v_3} J_0(Z_\infty \varrho_s) - Z_\infty G_R(\boldsymbol{x},\boldsymbol{y}) + \frac{Z_\infty}{2\pi|\boldsymbol{y}-\bar{\boldsymbol{x}}|}, \tag{4.114}$$

where G_R is computed according to (4.112). The derivatives for the variables y_1 and y_2 can be calculated by means of

$$\frac{\partial G}{\partial y_1} = \frac{\partial G}{\partial \varrho_s}\frac{\partial \varrho_s}{\partial y_1} = \frac{\partial G}{\partial \varrho_s}\frac{v_1}{\varrho_s} \qquad \text{and} \qquad \frac{\partial G}{\partial y_2} = \frac{\partial G}{\partial \varrho_s}\frac{\partial \varrho_s}{\partial y_2} = \frac{\partial G}{\partial \varrho_s}\frac{v_2}{\varrho_s}, \tag{4.115}$$

where

$$\begin{aligned}\frac{\partial G}{\partial \varrho_s}(\boldsymbol{x},\boldsymbol{y}) = {}& \frac{\varrho_s}{4\pi|\boldsymbol{y}-\boldsymbol{x}|^3} + \frac{\varrho_s}{4\pi|\boldsymbol{y}-\bar{\boldsymbol{x}}|^3} + \frac{iZ_\infty^2}{2}\, e^{-Z_\infty v_3} J_1(Z_\infty \varrho_s) \\ & - \frac{Z_\infty^2}{2\pi}\, e^{-Z_\infty v_3} J_1(Z_\infty \varrho_s) \ln\Big(Z_\infty v_3 + Z_\infty \sqrt{\varrho_s^2 + v_3^2} \Big) \\ & + \frac{Z_\infty}{2\pi}\, e^{-Z_\infty v_3} \frac{\varrho_s J_0(Z_\infty \varrho_s)}{\sqrt{\varrho_s^2 + v_3^2}\Big(v_3 + \sqrt{\varrho_s^2 + v_3^2} \Big)} \\ & - \frac{Z_\infty^2}{4}\, e^{-Z_\infty v_3} \left(Y_1(Z_\infty \varrho_s) - \frac{2}{\pi} J_1(Z_\infty \varrho_s) \ln(Z_\infty \varrho_s) + \frac{2}{\pi Z_\infty \varrho_s} J_0(Z_\infty \varrho_s) \right) \\ & + \frac{Z_\infty^2}{2\pi} \frac{\varrho_s}{\sqrt{\varrho_s^2 + v_3^2}}\, e^{-Z_\infty v_3} \Big(\mathrm{So}\big(Z_\infty \varrho_s, Z_\infty v_3\big) + \mathrm{Se}\big(Z_\infty \varrho_s, Z_\infty v_3\big) \Big) \\ & + \frac{Z_\infty^3}{2\pi} \sqrt{\varrho_s^2 + v_3^2}\, e^{-Z_\infty v_3} \left(\frac{\partial\, \mathrm{So}}{\partial \varrho_s}\big(Z_\infty \varrho_s, Z_\infty v_3\big) + \frac{\partial\, \mathrm{Se}}{\partial \varrho_s}\big(Z_\infty \varrho_s, Z_\infty v_3\big) \right), \end{aligned} \tag{4.116}$$

being

$$\frac{\partial\, \mathrm{So}}{\partial \varrho_s}(\varrho_s, v_3) = \sum_{n=0}^{\infty} \sum_{m=1}^{\infty} (-1)^m \frac{m\, 2^{2n+1} (n!)^2\, v_3^{2n+1} \varrho_s^{2m-1}}{(2n+1)!\, 2^{2(m+n+1)} \big((m+n+1)!\big)^2}, \tag{4.117}$$

$$\frac{\partial\, \mathrm{Se}}{\partial \varrho_s}(\varrho_s, v_3) = \sum_{n=0}^{\infty} \sum_{m=1}^{\infty} (-1)^m \frac{m\,(2n)!}{2^{2n-1}(n!)^2} \left(\frac{2^{m+n}(m+n)!}{(2n+2m+1)!} \right)^2 v_3^{2n} \varrho_s^{2m-1}. \tag{4.118}$$

4.3.5 Extension and properties

The half-space Green's function can be extended in a locally analytic way towards the full-space $\mathbb{R}^3$ in a straightforward and natural manner, just by considering the expression (4.113) valid for all $\boldsymbol{x}, \boldsymbol{y} \in \mathbb{R}^3$, instead of just for $\mathbb{R}^3_+$. As shown in Figure 4.8, this extension possesses two pole-type singularities at the points $\boldsymbol{x}$ and $\bar{\boldsymbol{x}}$, a logarithmic singularity-distribution along the half-line $\Upsilon = \{y_1 = x_1,\, y_2 = x_2,\, y_3 < -x_3\}$, and is continuous otherwise. The behavior of the pole-type singularities is characterized by

$$G(\boldsymbol{x},\boldsymbol{y}) \sim -\frac{1}{4\pi|\boldsymbol{y}-\boldsymbol{x}|}, \qquad \boldsymbol{y} \longrightarrow \boldsymbol{x}, \tag{4.119}$$

$$G(\boldsymbol{x},\boldsymbol{y}) \sim -\frac{1}{4\pi|\boldsymbol{y}-\bar{\boldsymbol{x}}|}, \qquad \boldsymbol{y} \longrightarrow \bar{\boldsymbol{x}}. \tag{4.120}$$

The logarithmic singularity-distribution stems from the fact that when $v_3 < 0$, then

$$G(\boldsymbol{x},\boldsymbol{y}) \sim -\frac{iZ_\infty}{2}\, e^{-Z_\infty v_3} H_0^{(1)}(Z_\infty \varrho_s), \tag{4.121}$$

being $H_0^{(1)}$ the zeroth order Hankel function of the first kind, whose singularity is of logarithmic type. We observe that (4.121) is related to the two-dimensional free-space Green's function of the Helmholtz equation (C.22), multiplied by the exponential weight

$$J(\boldsymbol{x},\boldsymbol{y}) = 2Z_\infty e^{-Z_\infty v_3}. \tag{4.122}$$

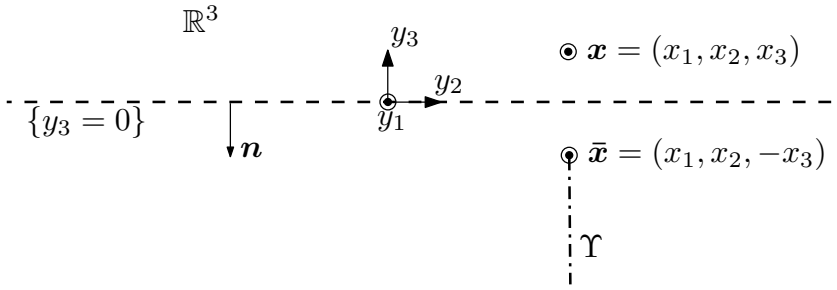

FIGURE 4.8. Domain of the extended Green's function.

As long as $x_3 \neq 0$, it is clear that the impedance boundary condition in (4.16) continues to be homogeneous. Nonetheless, if the source point $\boldsymbol{x}$ lies on the half-space's boundary, i.e., if $x_3 = 0$, then the boundary condition ceases to be homogeneous in the sense of distributions. This can be deduced from the expression (4.77) by verifying that

$$\lim_{y_3 \to 0^+} \left\{ \frac{\partial G}{\partial y_3}\big((\boldsymbol{x}_s, 0), \boldsymbol{y}\big) + Z_\infty G\big((\boldsymbol{x}_s, 0), \boldsymbol{y}\big) \right\} = \delta_{\boldsymbol{x}_s}(\boldsymbol{y}_s), \tag{4.123}$$

where $\boldsymbol{x}_s = (x_1, x_2)$ and $\boldsymbol{y}_s = (y_1, y_2)$. Since the impedance boundary condition holds only on $\{y_3 = 0\}$, therefore the right-hand side of (4.123) can be also expressed by

$$\delta_{\boldsymbol{x}_s}(\boldsymbol{y}_s) = \frac{1}{2}\delta_{\boldsymbol{x}}(\boldsymbol{y}) + \frac{1}{2}\delta_{\bar{\boldsymbol{x}}}(\boldsymbol{y}), \tag{4.124}$$

which illustrates more clearly the contribution of each pole-type singularity to the Dirac mass in the boundary condition.

It can be seen now that the Green's function extended in the abovementioned way satisfies, for $\boldsymbol{x} \in \mathbb{R}^3$, in the sense of distributions, and instead of (4.16), the problem

$$\begin{cases} \text{Find } G(\boldsymbol{x}, \cdot) : \mathbb{R}^3 \to \mathbb{C} \text{ such that} \\ \Delta_{\boldsymbol{y}} G(\boldsymbol{x}, \boldsymbol{y}) = \delta_{\boldsymbol{x}}(\boldsymbol{y}) + \delta_{\bar{\boldsymbol{x}}}(\boldsymbol{y}) + J(\boldsymbol{x}, \boldsymbol{y})\delta_\Upsilon(\boldsymbol{y}) \qquad \text{in } \mathcal{D}'(\mathbb{R}^3), \\ \dfrac{\partial G}{\partial y_3}(\boldsymbol{x}, \boldsymbol{y}) + Z_\infty G(\boldsymbol{x}, \boldsymbol{y}) = \dfrac{1}{2}\delta_{\boldsymbol{x}}(\boldsymbol{y}) + \dfrac{1}{2}\delta_{\bar{\boldsymbol{x}}}(\boldsymbol{y}) \qquad \text{on } \{y_3 = 0\}, \\ + \text{ Outgoing radiation condition for } \boldsymbol{y} \in \mathbb{R}^3_+ \text{ as } |\boldsymbol{y}| \to \infty, \end{cases} \tag{4.125}$$

where δ_Υ denotes a Dirac mass distribution along the Υ-curve. We retrieve thus the known result that for an impedance boundary condition the image of a point source is a point source plus a half-line of sources with exponentially increasing strengths in the lower half-plane, and which extends from the image point source towards infinity along the half-space's normal direction (cf. Keller 1979, who refers to decreasing strengths when dealing with the opposite half-space).

We note that the half-space Green's function (4.113) is symmetric in the sense that

$$G(\boldsymbol{x}, \boldsymbol{y}) = G(\boldsymbol{y}, \boldsymbol{x}) \qquad \forall \boldsymbol{x}, \boldsymbol{y} \in \mathbb{R}^3, \tag{4.126}$$

and it fulfills similarly

$$\nabla_{\boldsymbol{y}} G(\boldsymbol{x}, \boldsymbol{y}) = \nabla_{\boldsymbol{y}} G(\boldsymbol{y}, \boldsymbol{x}) \qquad \text{and} \qquad \nabla_{\boldsymbol{x}} G(\boldsymbol{x}, \boldsymbol{y}) = \nabla_{\boldsymbol{x}} G(\boldsymbol{y}, \boldsymbol{x}). \tag{4.127}$$

Another property is that we retrieve the special case (4.19) of a homogenous Dirichlet boundary condition in $\mathbb{R}^3_+$ when $Z_\infty \to \infty$. Likewise, we retrieve the special case (4.21) of a homogenous Neumann boundary condition in $\mathbb{R}^3_+$ when $Z_\infty \to 0$.

At last, we observe that the expression for the Green's function (4.113) is still valid if a complex impedance $Z_\infty \in \mathbb{C}$ such that $\mathfrak{Im}\{Z_\infty\} > 0$ and $\mathfrak{Re}\{Z_\infty\} \geq 0$ is used, which holds also for its derivatives (4.115), and (4.116).

4.4 Far field of the Green's function

4.4.1 Decomposition of the far field

The far field of the Green's function, which we denote by G^{ff}, describes its asymptotic behavior at infinity, i.e., when $|\boldsymbol{x}| \to \infty$ and assuming that $\boldsymbol{y}$ is fixed. For this purpose, the terms of highest order at infinity are searched. Likewise as done for the radiation condition, the far field is decomposed into two parts, each acting on a different region. The first part, denoted by G^{ff}_A, is linked with the asymptotic decaying condition at infinity observed when dealing with bounded obstacles, and acts in the interior of the half-space while vanishing near its boundary. The second part, denoted by G^{ff}_S, is associated with surface waves that propagate along the boundary towards infinity, which decay exponentially towards the half-space's interior. We have thus that

$$G^{ff} = G^{ff}_A + G^{ff}_S. \tag{4.128}$$

4.4.2 Asymptotic decaying

The asymptotic decaying acts only in the interior of the half-space and is related to the pole-type terms in (4.113), and also to the asymptotic behavior as $x_3 \to \infty$ of the remaining terms. We remember that

$$G(\boldsymbol{x},\boldsymbol{y}) = -\frac{1}{4\pi|\boldsymbol{x}-\boldsymbol{y}|} - \frac{1}{4\pi|\boldsymbol{x}-\bar{\boldsymbol{y}}|} - \frac{iZ_\infty}{2}\, e^{-Z_\infty v_3} J_0(Z_\infty \varrho_s) + G_R(\boldsymbol{x},\boldsymbol{y}), \tag{4.129}$$

being $\bar{\boldsymbol{y}} = (y_1, y_2, -y_3)$, and where different expressions for G_R were already presented in (4.86), (4.99), and (4.112). Due the axial symmetry around the axis $\{\varrho_s = 0\}$, i.e., by using the same arguments as for (4.65), we can express the inverse Fourier transform of (4.76) as

$$G_R(\boldsymbol{x},\boldsymbol{y}) = \frac{Z_\infty}{4\pi^2} \int_0^\pi \int_{-\infty}^\infty \frac{e^{-|\xi| v_3}}{Z_\infty - |\xi|}\, e^{i\xi\varrho_s \sin\psi}\, \mathrm{d}\xi\, \mathrm{d}\psi. \tag{4.130}$$

This integral can be rewritten as

$$G_R(\boldsymbol{x},\boldsymbol{y}) = \frac{Z_\infty}{\pi^2} \int_0^{\pi/2} \int_0^\infty \frac{e^{-\rho v_3}}{Z_\infty - \rho} \cos\big(\rho\varrho_s \sin\psi\big)\, \mathrm{d}\rho\, \mathrm{d}\psi. \tag{4.131}$$

The innermost integral in (4.131) is the same as the one that appears for the two-dimensional case in (2.80), and can be computed in the same way. It corresponds to exponential integral functions Ei (vid. Subsection A.2.3). By comparing (2.80) and (2.93), and by performing a change of variables on the second term to account for a sign difference, we obtain the

integral representation

$$G_R(\boldsymbol{x},\boldsymbol{y}) = \frac{Z_\infty}{2\pi^2}\, e^{-Z_\infty v_3} \int_{-\pi/2}^{\pi/2} e^{iZ_\infty \varrho_s \sin\psi}\, \mathrm{Ei}\big(Z_\infty v_3 - iZ_\infty \varrho_s \sin\psi\big)\, \mathrm{d}\psi, \tag{4.132}$$

which can be rewritten also as

$$G_R(\boldsymbol{x},\boldsymbol{y}) = \frac{Z_\infty}{2\pi^2} \int_{-1}^{1} \frac{e^{-Z_\infty(v_3 - i\varrho_s\eta)}}{\sqrt{1-\eta^2}}\, \mathrm{Ei}\big(Z_\infty(v_3 - i\varrho_s\eta)\big)\, \mathrm{d}\eta. \tag{4.133}$$

Now, as $x_3 \to \infty$, we can consider the asymptotic behavior of the exponential integral in (4.133). In fact, due (A.81) we have for $z \in \mathbb{C}$ that

$$\mathrm{Ei}(z) \sim \frac{e^z}{z} \qquad \text{as } \ \mathfrak{Re}\{z\} \to \infty. \tag{4.134}$$

Hence, as $x_3 \to \infty$ it holds that

$$G_R(\boldsymbol{x},\boldsymbol{y}) \sim \frac{1}{2\pi^2} \int_{-1}^{1} \frac{\mathrm{d}\eta}{(v_3 - i\varrho_s\eta)\sqrt{1-\eta^2}} = \frac{1}{2\pi|\boldsymbol{x}-\bar{\boldsymbol{y}}|}. \tag{4.135}$$

The Green's function (4.129) behaves thus asymptotically, when $x_3 \to \infty$, as

$$G(\boldsymbol{x},\boldsymbol{y}) \sim -\frac{1}{4\pi|\boldsymbol{x}-\boldsymbol{y}|} + \frac{1}{4\pi|\boldsymbol{x}-\bar{\boldsymbol{y}}|}. \tag{4.136}$$

By using Taylor expansions as in (D.29), we obtain that

$$-\frac{1}{4\pi|\boldsymbol{x}-\boldsymbol{y}|} + \frac{1}{4\pi|\boldsymbol{x}-\bar{\boldsymbol{y}}|} = -\frac{(\boldsymbol{y}-\bar{\boldsymbol{y}})\cdot\boldsymbol{x}}{4\pi|\boldsymbol{x}|^3} + \mathcal{O}\bigg(\frac{1}{|\boldsymbol{x}|^3}\bigg). \tag{4.137}$$

We express the point $\boldsymbol{x}$ as $\boldsymbol{x} = |\boldsymbol{x}|\,\hat{\boldsymbol{x}}$, being $\hat{\boldsymbol{x}} = (\sin\theta\cos\varphi, \sin\theta\sin\varphi, \cos\theta)$ a vector of the unit sphere. The asymptotic decaying of the Green's function is therefore given by

$$G_A^{ff}(\boldsymbol{x},\boldsymbol{y}) = -\frac{y_3\cos\theta}{2\pi|\boldsymbol{x}|^2}, \tag{4.138}$$

and its gradient with respect to $\boldsymbol{y}$ by

$$\nabla_{\boldsymbol{y}} G_A^{ff}(\boldsymbol{x},\boldsymbol{y}) = -\frac{\cos\theta}{2\pi|\boldsymbol{x}|^2} \begin{bmatrix} 0 \\ 0 \\ 1 \end{bmatrix}. \tag{4.139}$$

4.4.3 Surface waves in the far field

An expression for the surface waves in the far field can be obtained by studying the residues of the poles of the spectral Green's function, which determine entirely their asymptotic behavior. We already computed the inverse Fourier transform of these residues in (4.66), using the residue theorem of Cauchy and the limiting absorption principle. This implies that the Green's function behaves asymptotically, when $|\boldsymbol{x}_s| \to \infty$, as

$$G(\boldsymbol{x},\boldsymbol{y}) \sim -\frac{iZ_\infty}{2}\, e^{-Z_\infty v_3} \Big[J_0(Z_\infty \varrho_s) + i\boldsymbol{H}_0(Z_\infty \varrho_s)\Big] \qquad \text{for } \ v_3 > 0. \tag{4.140}$$

This expression works well in the upper half-space, but fails to retrieve the logarithmic singularity-distribution (4.121) in the lower half-space at $\varrho_s = 0$. In this case, the Struve function $\boldsymbol{H}_0$ in (4.140) has to be replaced by the Neumann function Y_0, which has the same

behavior at infinity, but additionally a logarithmic singularity at its origin. Hence in the lower half-space, the Green's function behaves asymptotically, when $|\boldsymbol{x}_s| \to \infty$, as

$$G(\boldsymbol{x},\boldsymbol{y}) \sim -\frac{iZ_\infty}{2}\, e^{-Z_\infty v_3} H_0^{(1)}(Z_\infty \varrho_s) \qquad \text{for } \; v_3 < 0. \tag{4.141}$$

In general, away from the axis $\{\varrho_s = 0\}$, the Green's function behaves, when $|\boldsymbol{x}_s| \to \infty$ and due the asymptotic expansions of the Struve and Bessel functions, as

$$G(\boldsymbol{x},\boldsymbol{y}) \sim -i\sqrt{\frac{Z_\infty}{2\pi\varrho_s}}\, e^{-Z_\infty v_3} e^{i(Z_\infty \varrho_s - \pi/4)}. \tag{4.142}$$

By performing Taylor expansions, as in (C.37) and (C.38), we have that

$$\frac{e^{iZ_\infty \varrho_s}}{\sqrt{\varrho_s}} = \frac{e^{iZ_\infty |\boldsymbol{x}_s|}}{\sqrt{|\boldsymbol{x}_s|}}\, e^{-iZ_\infty \boldsymbol{y}_s\cdot\boldsymbol{x}_s/|\boldsymbol{x}_s|} \left(1 + \mathcal{O}\Big(\frac{1}{|\boldsymbol{x}_s|}\Big)\right). \tag{4.143}$$

We express the point $\boldsymbol{x}_s$ on the surface as $\boldsymbol{x}_s = |\boldsymbol{x}_s|\,\hat{\boldsymbol{x}}_s$, being $\hat{\boldsymbol{x}}_s = (\cos\varphi, \sin\varphi)$ a unitary surface vector. The surface-wave behavior of the Green's function, due (4.142) and (4.143), becomes thus

$$G_S^{ff}(\boldsymbol{x},\boldsymbol{y}) = -i\, e^{-i\pi/4}\sqrt{\frac{Z_\infty}{2\pi|\boldsymbol{x}_s|}}\, e^{-Z_\infty x_3} e^{iZ_\infty|\boldsymbol{x}_s|} e^{-Z_\infty y_3} e^{-iZ_\infty \boldsymbol{y}_s\cdot\hat{\boldsymbol{x}}_s}, \tag{4.144}$$

and its gradient with respect to $\boldsymbol{y}$ is given by

$$\nabla_{\boldsymbol{y}} G_S^{ff}(\boldsymbol{x},\boldsymbol{y}) = -\frac{Z_\infty^{3/2}}{\sqrt{2\pi|\boldsymbol{x}_s|}}\, e^{-i\pi/4} e^{-Z_\infty x_3} e^{iZ_\infty|\boldsymbol{x}_s|} e^{-Z_\infty y_3} e^{-iZ_\infty \boldsymbol{y}_s\cdot\hat{\boldsymbol{x}}_s} \begin{bmatrix} \cos\varphi \\ \sin\varphi \\ -i \end{bmatrix}. \tag{4.145}$$

4.4.4 Complete far field of the Green's function

On the whole, the asymptotic behavior of the Green's function as $|\boldsymbol{x}| \to \infty$ can be characterized in the upper half-space through the addition of (4.136) and (4.140), and in the lower half-space by adding (4.136) and (4.141). Thus if $v_3 > 0$, then it holds that

$$G(\boldsymbol{x},\boldsymbol{y}) \sim -\frac{1}{4\pi|\boldsymbol{x}-\boldsymbol{y}|} + \frac{1}{4\pi|\boldsymbol{x}-\bar{\boldsymbol{y}}|} - \frac{iZ_\infty}{2}\, e^{-Z_\infty v_3}\Big[J_0(Z_\infty\varrho_s) + i\boldsymbol{H}_0(Z_\infty\varrho_s)\Big], \tag{4.146}$$

and if $v_3 < 0$, then

$$G(\boldsymbol{x},\boldsymbol{y}) \sim -\frac{1}{4\pi|\boldsymbol{x}-\boldsymbol{y}|} + \frac{1}{4\pi|\boldsymbol{x}-\bar{\boldsymbol{y}}|} - \frac{iZ_\infty}{2}\, e^{-Z_\infty v_3} H_0^{(1)}(Z_\infty\varrho_s). \tag{4.147}$$

Consequently, the complete far field of the Green's function, due (4.128), should be given by the addition of (4.138) and (4.144), i.e., by

$$G^{ff}(\boldsymbol{x},\boldsymbol{y}) = -\frac{y_3\cos\theta}{2\pi|\boldsymbol{x}|^2} - i\, e^{-i\pi/4}\sqrt{\frac{Z_\infty}{2\pi|\boldsymbol{x}_s|}}\, e^{-Z_\infty x_3} e^{iZ_\infty|\boldsymbol{x}_s|} e^{-Z_\infty y_3} e^{-iZ_\infty \boldsymbol{y}_s\cdot\hat{\boldsymbol{x}}_s}. \tag{4.148}$$

Its derivative with respect to $\boldsymbol{y}$ is likewise given by the addition of (4.139) and (4.145). The expression (4.148) retrieves correctly the far field of the Green's function, except in the upper half-space at the vicinity of the axis $\{\varrho_s = 0\}$, due the presence of a singularity-distribution of type $1/\sqrt{|\boldsymbol{x}_s|}$, which does not appear in the original Green's function. A

way to deal with this issue is to consider in each region only the most dominant asymptotic behavior at infinity. Since there are two different regions, we require to determine appropriately the interface between them. This can be achieved by equating the amplitudes of the two terms in (4.148), i.e., by searching values of $\boldsymbol{x}$ at infinity such that

$$\frac{1}{2\pi|\boldsymbol{x}|^2} = \sqrt{\frac{Z_\infty}{2\pi|\boldsymbol{x}|}}\, e^{-Z_\infty x_3}, \tag{4.149}$$

where we neglected the values of $\boldsymbol{y}$, since they remain relatively near the origin. Furthermore, since the interface stays relatively close to the half-space's boundary, we can also approximate $|\boldsymbol{x}_s| \approx |\boldsymbol{x}|$. By taking the logarithm in (4.149) and perturbing somewhat the result so as to avoid a singular behavior at the origin, we obtain finally that this interface is described by

$$x_3 = \frac{1}{2Z_\infty} \ln\bigl(1 + 2\pi Z_\infty |\boldsymbol{x}|^3\bigr). \tag{4.150}$$

We can say now that it is the far field (4.148) which justifies the radiation condition (4.17) when exchanging the roles of $\boldsymbol{x}$ and $\boldsymbol{y}$, and disregarding the undesired singularity around $\{\varrho_s = 0\}$. When the first term in (4.148) dominates, i.e., the asymptotic decaying (4.138), then it is the first expression in (4.17) that matters. Conversely, when the second term in (4.148) dominates, i.e., the surface waves (4.144), then the second expression in (4.17) is the one that holds. The interface between both is described by (4.150).

We remark that the asymptotic behavior (4.146) of the Green's function and the expression (4.148) of its complete far field do no longer hold if a complex impedance $Z_\infty \in \mathbb{C}$ such that $\mathfrak{Im}\{Z_\infty\} > 0$ and $\mathfrak{Re}\{Z_\infty\} \geq 0$ is used, specifically the parts (4.140) and (4.144) linked with the surface waves. A careful inspection shows that in this case the surface-wave behavior of the Green's function, as $|\boldsymbol{x}_s| \to \infty$, decreases exponentially and is given by

$$G(\boldsymbol{x}, \boldsymbol{y}) \sim -\frac{iZ_\infty}{2}\, e^{-|Z_\infty| v_3} \Bigl[J_0(Z_\infty \varrho_s) + i\boldsymbol{H}_0(Z_\infty \varrho_s) \Bigr] \qquad \text{for } \; v_3 > 0, \tag{4.151}$$

whereas (4.141) continues to hold. Likewise, the surface-wave part of the far field is expressed for $x_3 > 0$ as

$$G_S^{ff}(\boldsymbol{x}, \boldsymbol{y}) = -i\, e^{-i\pi/4} \sqrt{\frac{Z_\infty}{2\pi|\boldsymbol{x}_s|}}\, e^{-|Z_\infty| x_3} e^{iZ_\infty |\boldsymbol{x}_s|} e^{-|Z_\infty| y_3} e^{-iZ_\infty \boldsymbol{y}_s \cdot \hat{\boldsymbol{x}}_s}, \tag{4.152}$$

but for $x_3 < 0$ the expression (4.144) is still valid. The asymptotic decaying (4.136) and its far-field expression (4.138), on the other hand, remain the same when we use a complex impedance. We remark further that if a complex impedance is taken into account, then the part of the surface waves of the outgoing radiation condition is redundant, and only the asymptotic decaying part is required, i.e., only the first two expressions in (4.17), but now holding for $y_3 > 0$.

4.5 Numerical evaluation of the Green's function

For the numerical evaluation of the Green's function, we separate the space $\mathbb{R}^3$ into three regions: a near field, an upper far field, and a lower far field. In the near field,

when $|Z_\infty|\,|\boldsymbol{v}| \leq 15$, being $\boldsymbol{v} = \boldsymbol{y} - \bar{\boldsymbol{x}}$, we use the expression (4.113) to compute the Green's function, truncating the double series of the functions So and Se, in (4.109) and (4.110) respectively, after the first 30 terms for n and m. In the upper far field, when $|Z_\infty|\,|\boldsymbol{v}| > 15$ and $|Z_\infty|\,v_3 > \log\big(1 + 2\pi|Z_\infty|\varrho_s^3\big)$, we have from (4.146) that

$$G(\boldsymbol{x},\boldsymbol{y}) = -\frac{1}{4\pi|\boldsymbol{x}-\boldsymbol{y}|} + \frac{1}{4\pi|\boldsymbol{x}-\bar{\boldsymbol{y}}|} - \frac{iZ_\infty}{2}\, e^{-Z_\infty v_3}\Big[J_0(Z_\infty\varrho_s) + i\boldsymbol{H}_0(Z_\infty\varrho_s)\Big]. \quad (4.153)$$

Similarly in the lower far field, when $|Z_\infty|\,|\boldsymbol{v}| > 15$ and $|Z_\infty|\,v_3 \leq \log\big(1 + 2\pi|Z_\infty|\varrho_s^3\big)$, it holds from (4.147) that

$$G(\boldsymbol{x},\boldsymbol{y}) = -\frac{1}{4\pi|\boldsymbol{x}-\boldsymbol{y}|} + \frac{1}{4\pi|\boldsymbol{x}-\bar{\boldsymbol{y}}|} - \frac{iZ_\infty}{2}\, e^{-Z_\infty v_3} H_0^{(1)}(Z_\infty\varrho_s). \quad (4.154)$$

The Bessel functions can be evaluated either by using the software based on the technical report by Morris (1993) or the subroutines described in Amos (1986, 1995). The Struve function can be computed by means of the software described in MacLeod (1996). Further references are listed in Lozier & Olver (1994). The biggest numerical error, excepting the singularity-distribution along the half-line Υ, is committed near the boundaries of the three described regions, and amounts to less than $|Z_\infty| \cdot 10^{-3}$.

4.6 Integral representation and equation

4.6.1 Integral representation

We are interested in expressing the solution u of the direct scattering problem (4.13) by means of an integral representation formula over the perturbed portion of the boundary Γ_p. For this purpose, we extend this solution by zero towards the complementary domain Ω_c, analogously as done in (D.98). We define by $\Omega_{R,\varepsilon}$ the domain Ω_e without the ball B_ε of radius $\varepsilon > 0$ centered at the point $\boldsymbol{x} \in \Omega_e$, and truncated at infinity by the ball B_R of radius $R > 0$ centered at the origin. We consider that the ball B_ε is entirely contained in Ω_e. Therefore, as shown in Figure 4.9, we have that

$$\Omega_{R,\varepsilon} = \big(\Omega_e \cap B_R\big) \setminus \overline{B_\varepsilon}, \quad (4.155)$$

where

$$B_R = \{\boldsymbol{y} \in \mathbb{R}^3 :\, |\boldsymbol{y}| < R\} \qquad \text{and} \qquad B_\varepsilon = \{\boldsymbol{y} \in \Omega_e :\, |\boldsymbol{y}-\boldsymbol{x}| < \varepsilon\}. \quad (4.156)$$

We consider similarly, inside Ω_e, the boundaries of the balls

$$S_R^+ = \{\boldsymbol{y} \in \mathbb{R}^3_+ :\, |\boldsymbol{y}| = R\} \qquad \text{and} \qquad S_\varepsilon = \{\boldsymbol{y} \in \Omega_e :\, |\boldsymbol{y}-\boldsymbol{x}| = \varepsilon\}. \quad (4.157)$$

We separate furthermore the boundary as $\Gamma = \Gamma_0 \cup \Gamma_+$, where

$$\Gamma_0 = \{\boldsymbol{y} \in \Gamma :\, y_3 = 0\} \qquad \text{and} \qquad \Gamma_+ = \{\boldsymbol{y} \in \Gamma :\, y_3 > 0\}. \quad (4.158)$$

The boundary Γ is likewise truncated at infinity by the ball B_R, namely

$$\Gamma_R = \Gamma \cap B_R = \Gamma_0^R \cup \Gamma_+ = \Gamma_\infty^R \cup \Gamma_p, \quad (4.159)$$

where

$$\Gamma_0^R = \Gamma_0 \cap B_R \qquad \text{and} \qquad \Gamma_\infty^R = \Gamma_\infty \cap B_R. \quad (4.160)$$

The idea is to retrieve the domain Ω_e and the boundary Γ at the end when the limits $R \to \infty$ and $\varepsilon \to 0$ are taken for the truncated domain $\Omega_{R,\varepsilon}$ and the truncated boundary Γ_R.

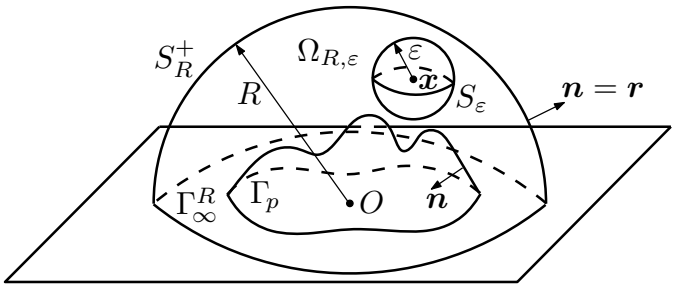

FIGURE 4.9. Truncated domain $\Omega_{R,\varepsilon}$ for $\boldsymbol{x} \in \Omega_e$.

We apply now Green's second integral theorem (A.613) to the functions u and $G(\boldsymbol{x}, \cdot)$ in the bounded domain $\Omega_{R,\varepsilon}$, yielding

$$\begin{aligned} 0 &= \int_{\Omega_{R,\varepsilon}} \big(u(\boldsymbol{y})\Delta_{\boldsymbol{y}} G(\boldsymbol{x},\boldsymbol{y}) - G(\boldsymbol{x},\boldsymbol{y})\Delta u(\boldsymbol{y})\big)\mathrm{d}\boldsymbol{y} \\ &= \int_{S_R^+} \left(u(\boldsymbol{y})\frac{\partial G}{\partial r_{\boldsymbol{y}}}(\boldsymbol{x},\boldsymbol{y}) - G(\boldsymbol{x},\boldsymbol{y})\frac{\partial u}{\partial r}(\boldsymbol{y})\right)\mathrm{d}\gamma(\boldsymbol{y}) \\ &- \int_{S_\varepsilon} \left(u(\boldsymbol{y})\frac{\partial G}{\partial r_{\boldsymbol{y}}}(\boldsymbol{x},\boldsymbol{y}) - G(\boldsymbol{x},\boldsymbol{y})\frac{\partial u}{\partial r}(\boldsymbol{y})\right)\mathrm{d}\gamma(\boldsymbol{y}) \\ &+ \int_{\Gamma_R} \left(u(\boldsymbol{y})\frac{\partial G}{\partial n_{\boldsymbol{y}}}(\boldsymbol{x},\boldsymbol{y}) - G(\boldsymbol{x},\boldsymbol{y})\frac{\partial u}{\partial n}(\boldsymbol{y})\right)\mathrm{d}\gamma(\boldsymbol{y}). \end{aligned} \tag{4.161}$$

The integral on S_R^+ can be rewritten as

$$\begin{aligned} \int_{S_R^2} \left[u(\boldsymbol{y})\left(\frac{\partial G}{\partial r_{\boldsymbol{y}}}(\boldsymbol{x},\boldsymbol{y}) - iZ_\infty G(\boldsymbol{x},\boldsymbol{y})\right) - G(\boldsymbol{x},\boldsymbol{y})\left(\frac{\partial u}{\partial r}(\boldsymbol{y}) - iZ_\infty u(\boldsymbol{y})\right)\right]\mathrm{d}\gamma(\boldsymbol{y}) \\ + \int_{S_R^1} \left(u(\boldsymbol{y})\frac{\partial G}{\partial r_{\boldsymbol{y}}}(\boldsymbol{x},\boldsymbol{y}) - G(\boldsymbol{x},\boldsymbol{y})\frac{\partial u}{\partial r}(\boldsymbol{y})\right)\mathrm{d}\gamma(\boldsymbol{y}), \end{aligned} \tag{4.162}$$

which for R large enough and due the radiation condition (4.6) tends to zero, since

$$\left|\int_{S_R^2} u(\boldsymbol{y})\left(\frac{\partial G}{\partial r_{\boldsymbol{y}}}(\boldsymbol{x},\boldsymbol{y}) - iZ_\infty G(\boldsymbol{x},\boldsymbol{y})\right)\mathrm{d}\gamma(\boldsymbol{y})\right| \leq \frac{C}{\sqrt{R}}\ln R, \tag{4.163}$$

$$\left|\int_{S_R^2} G(\boldsymbol{x},\boldsymbol{y})\left(\frac{\partial u}{\partial r}(\boldsymbol{y}) - iZ_\infty u(\boldsymbol{y})\right)\mathrm{d}\gamma(\boldsymbol{y})\right| \leq \frac{C}{\sqrt{R}}\ln R, \tag{4.164}$$

and

$$\left|\int_{S_R^1} \left(u(\boldsymbol{y})\frac{\partial G}{\partial r_{\boldsymbol{y}}}(\boldsymbol{x},\boldsymbol{y}) - G(\boldsymbol{x},\boldsymbol{y})\frac{\partial u}{\partial r}(\boldsymbol{y})\right)\mathrm{d}\gamma(\boldsymbol{y})\right| \leq \frac{C}{R^3}, \tag{4.165}$$

for some constants $C > 0$. If the function u is regular enough in the ball B_ε, then the second term of the integral on S_ε in (4.161), when $\varepsilon \to 0$ and due (4.119), is bounded by

$$\left| \int_{S_\varepsilon} G(\boldsymbol{x}, \boldsymbol{y}) \frac{\partial u}{\partial r}(\boldsymbol{y}) \, \mathrm{d}\gamma(\boldsymbol{y}) \right| \leq C\varepsilon \sup_{\boldsymbol{y} \in B_\varepsilon} \left| \frac{\partial u}{\partial r}(\boldsymbol{y}) \right|, \tag{4.166}$$

for some constant $C > 0$ and tends to zero. The regularity of u can be specified afterwards once the integral representation has been determined and generalized by means of density arguments. The first integral term on S_ε can be decomposed as

$$\begin{aligned} \int_{S_\varepsilon} u(\boldsymbol{y}) \frac{\partial G}{\partial r_{\boldsymbol{y}}}(\boldsymbol{x}, \boldsymbol{y}) \, \mathrm{d}\gamma(\boldsymbol{y}) = u(\boldsymbol{x}) \int_{S_\varepsilon} \frac{\partial G}{\partial r_{\boldsymbol{y}}}(\boldsymbol{x}, \boldsymbol{y}) \, \mathrm{d}\gamma(\boldsymbol{y}) \\ + \int_{S_\varepsilon} \frac{\partial G}{\partial r_{\boldsymbol{y}}}(\boldsymbol{x}, \boldsymbol{y}) \big(u(\boldsymbol{y}) - u(\boldsymbol{x}) \big) \, \mathrm{d}\gamma(\boldsymbol{y}), \end{aligned} \tag{4.167}$$

For the first term in the right-hand side of (4.167), by considering (4.119) we have that

$$\int_{S_\varepsilon} \frac{\partial G}{\partial r_{\boldsymbol{y}}}(\boldsymbol{x}, \boldsymbol{y}) \, \mathrm{d}\gamma(\boldsymbol{y}) \quad \xrightarrow[\varepsilon \to 0]{} \quad 1, \tag{4.168}$$

while the second term is bounded by

$$\left| \int_{S_\varepsilon} \big(u(\boldsymbol{y}) - u(\boldsymbol{x}) \big) \frac{\partial G}{\partial r_{\boldsymbol{y}}}(\boldsymbol{x}, \boldsymbol{y}) \, \mathrm{d}\gamma(\boldsymbol{y}) \right| \leq \sup_{\boldsymbol{y} \in B_\varepsilon} |u(\boldsymbol{y}) - u(\boldsymbol{x})|, \tag{4.169}$$

which tends towards zero when $\varepsilon \to 0$. Finally, due the impedance boundary condition (4.4) and since the support of f_z vanishes on Γ_∞, the term on Γ_R in (4.161) can be decomposed as

$$\begin{aligned} \int_{\Gamma_p} \left(\frac{\partial G}{\partial n_{\boldsymbol{y}}}(\boldsymbol{x}, \boldsymbol{y}) - Z(\boldsymbol{y}) G(\boldsymbol{x}, \boldsymbol{y}) \right) u(\boldsymbol{y}) \, \mathrm{d}\gamma(\boldsymbol{y}) + \int_{\Gamma_p} G(\boldsymbol{x}, \boldsymbol{y}) f_z(\boldsymbol{y}) \, \mathrm{d}\gamma(\boldsymbol{y}) \\ - \int_{\Gamma_\infty^R} \left(\frac{\partial G}{\partial y_2}(\boldsymbol{x}, \boldsymbol{y}) + Z_\infty G(\boldsymbol{x}, \boldsymbol{y}) \right) u(\boldsymbol{y}) \, \mathrm{d}\gamma(\boldsymbol{y}), \end{aligned} \tag{4.170}$$

where the integral on Γ_∞^R vanishes due the impedance boundary condition in (4.16). Therefore this term does not depend on R and has its support only on the bounded and perturbed portion Γ_p of the boundary.

In conclusion, when the limits $R \to \infty$ and $\varepsilon \to 0$ are taken in (4.161), then we obtain for $\boldsymbol{x} \in \Omega_e$ the integral representation formula

$$u(\boldsymbol{x}) = \int_{\Gamma_p} \left(\frac{\partial G}{\partial n_{\boldsymbol{y}}}(\boldsymbol{x}, \boldsymbol{y}) - Z(\boldsymbol{y}) G(\boldsymbol{x}, \boldsymbol{y}) \right) u(\boldsymbol{y}) \, \mathrm{d}\gamma(\boldsymbol{y}) + \int_{\Gamma_p} G(\boldsymbol{x}, \boldsymbol{y}) f_z(\boldsymbol{y}) \, \mathrm{d}\gamma(\boldsymbol{y}), \tag{4.171}$$

which can be alternatively expressed as

$$u(\boldsymbol{x}) = \int_{\Gamma_p} \left(u(\boldsymbol{y}) \frac{\partial G}{\partial n_{\boldsymbol{y}}}(\boldsymbol{x}, \boldsymbol{y}) - G(\boldsymbol{x}, \boldsymbol{y}) \frac{\partial u}{\partial n}(\boldsymbol{y}) \right) \mathrm{d}\gamma(\boldsymbol{y}). \tag{4.172}$$

It is remarkable in this integral representation that the support of the integral, namely the curve Γ_p, is bounded. Let us denote the traces of the solution and of its normal derivative

on Γ_p respectively by

$$\mu = u|_{\Gamma_p} \qquad \text{and} \qquad \nu = \left.\frac{\partial u}{\partial n}\right|_{\Gamma_p}. \tag{4.173}$$

We can rewrite now (4.171) and (4.172) in terms of layer potentials as

$$u = \mathcal{D}(\mu) - \mathcal{S}(Z\mu) + \mathcal{S}(f_z) \qquad \text{in } \Omega_e, \tag{4.174}$$

$$u = \mathcal{D}(\mu) - \mathcal{S}(\nu) \qquad \text{in } \Omega_e, \tag{4.175}$$

where we define for $\boldsymbol{x} \in \Omega_e$ respectively the single and double layer potentials as

$$\mathcal{S}\nu(\boldsymbol{x}) = \int_{\Gamma_p} G(\boldsymbol{x}, \boldsymbol{y})\nu(\boldsymbol{y})\,\mathrm{d}\gamma(\boldsymbol{y}), \tag{4.176}$$

$$\mathcal{D}\mu(\boldsymbol{x}) = \int_{\Gamma_p} \frac{\partial G}{\partial n_{\boldsymbol{y}}}(\boldsymbol{x}, \boldsymbol{y})\mu(\boldsymbol{y})\,\mathrm{d}\gamma(\boldsymbol{y}). \tag{4.177}$$

We remark that from the impedance boundary condition (4.4) it is clear that

$$\nu = Z\mu - f_z. \tag{4.178}$$

4.6.2 Integral equation

To determine entirely the solution of the direct scattering problem (4.13) by means of its integral representation, we have to find values for the traces (4.173). This requires the development of an integral equation that allows to fix these values by incorporating the boundary data. For this purpose we place the source point $\boldsymbol{x}$ on the boundary Γ and apply the same procedure as before for the integral representation (4.171), treating differently in (4.161) only the integrals on S_ε. The integrals on S_R^+ still behave well and tend towards zero as $R \to \infty$. The Ball B_ε, though, is split in half by the boundary Γ, and the portion $\Omega_e \cap B_\varepsilon$ is asymptotically separated from its complement in B_ε by the tangent of the boundary if Γ is regular. If $\boldsymbol{x} \in \Gamma_+$, then the associated integrals on S_ε give rise to a term $-u(\boldsymbol{x})/2$ instead of just $-u(\boldsymbol{x})$ as before for the integral representation. Therefore we obtain for $\boldsymbol{x} \in \Gamma_+$ the boundary integral representation

$$\frac{u(\boldsymbol{x})}{2} = \int_{\Gamma_p} \left(\frac{\partial G}{\partial n_{\boldsymbol{y}}}(\boldsymbol{x}, \boldsymbol{y}) - Z(\boldsymbol{y})G(\boldsymbol{x}, \boldsymbol{y}) \right) u(\boldsymbol{y})\,\mathrm{d}\gamma(\boldsymbol{y}) + \int_{\Gamma_p} G(\boldsymbol{x}, \boldsymbol{y}) f_z(\boldsymbol{y})\,\mathrm{d}\gamma(\boldsymbol{y}). \tag{4.179}$$

On the contrary, if $\boldsymbol{x} \in \Gamma_0$, then the pole-type behavior (4.120) contributes also to the singularity (4.119) of the Green's function and the integrals on S_ε give now rise to two terms $-u(\boldsymbol{x})/2$, i.e., on the whole to a term $-u(\boldsymbol{x})$. For $\boldsymbol{x} \in \Gamma_0$ the boundary integral representation is instead given by

$$u(\boldsymbol{x}) = \int_{\Gamma_p} \left(\frac{\partial G}{\partial n_{\boldsymbol{y}}}(\boldsymbol{x}, \boldsymbol{y}) - Z(\boldsymbol{y})G(\boldsymbol{x}, \boldsymbol{y}) \right) u(\boldsymbol{y})\,\mathrm{d}\gamma(\boldsymbol{y}) + \int_{\Gamma_p} G(\boldsymbol{x}, \boldsymbol{y}) f_z(\boldsymbol{y})\,\mathrm{d}\gamma(\boldsymbol{y}). \tag{4.180}$$

We must notice that in both cases, the integrands associated with the boundary Γ admit an integrable singularity at the point $\boldsymbol{x}$. In terms of boundary layer potentials, we can express these boundary integral representations as

$$\frac{u}{2} = D(\mu) - S(Z\mu) + S(f_z) \qquad \text{on } \Gamma_+, \tag{4.181}$$

$$u = D(\mu) - S(Z\mu) + S(f_z) \qquad \text{on } \Gamma_0, \tag{4.182}$$

where we consider, for $\boldsymbol{x} \in \Gamma$, the two boundary integral operators

$$S\nu(\boldsymbol{x}) = \int_{\Gamma_p} G(\boldsymbol{x}, \boldsymbol{y})\nu(\boldsymbol{y})\, \mathrm{d}\gamma(\boldsymbol{y}), \tag{4.183}$$

$$D\mu(\boldsymbol{x}) = \int_{\Gamma_p} \frac{\partial G}{\partial n_{\boldsymbol{y}}}(\boldsymbol{x}, \boldsymbol{y})\mu(\boldsymbol{y})\, \mathrm{d}\gamma(\boldsymbol{y}). \tag{4.184}$$

We can combine (4.181) and (4.182) into a single integral equation on Γ_p, namely

$$(1 + \mathcal{I}_0)\frac{\mu}{2} + S(Z\mu) - D(\mu) = S(f_z) \qquad \text{on } \Gamma_p, \tag{4.185}$$

where $\mathcal{I}_0$ denotes the characteristic or indicator function of the set Γ_0, i.e.,

$$\mathcal{I}_0(\boldsymbol{x}) = \begin{cases} 1 & \text{if } \boldsymbol{x} \in \Gamma_0, \\ 0 & \text{if } \boldsymbol{x} \notin \Gamma_0. \end{cases} \tag{4.186}$$

It is the solution μ on Γ_p of the integral equation (4.185) which finally allows to characterize the solution u in Ω_e of the direct scattering problem (4.13) through the integral representation formula (4.174). The trace of the solution u on the boundary Γ is then found simultaneously by means of the boundary integral representations (4.181) and (4.182). In particular, when $\boldsymbol{x} \in \Gamma_\infty$ and since $\Gamma_\infty \subset \Gamma_0$, therefore it holds that

$$u = D(\mu) - S(Z\mu) + S(f_z) \qquad \text{on } \Gamma_\infty. \tag{4.187}$$

4.7 Far field of the solution

The asymptotic behavior at infinity of the solution u of (4.13) is described by the far field. It is denoted by u^{ff} and is characterized by

$$u(\boldsymbol{x}) \sim u^{ff}(\boldsymbol{x}) \qquad \text{as } |\boldsymbol{x}| \to \infty. \tag{4.188}$$

Its expression can be deduced by replacing the far field of the Green's function G^{ff} and its derivatives in the integral representation formula (4.172), which yields

$$u^{ff}(\boldsymbol{x}) = \int_{\Gamma_p} \left(\frac{\partial G^{ff}}{\partial n_{\boldsymbol{y}}}(\boldsymbol{x}, \boldsymbol{y})\mu(\boldsymbol{y}) - G^{ff}(\boldsymbol{x}, \boldsymbol{y})\nu(\boldsymbol{y}) \right) \mathrm{d}\gamma(\boldsymbol{y}). \tag{4.189}$$

By replacing now (4.148) and the addition of (4.139) and (4.145) in (4.189), we obtain that

$$\begin{aligned} u^{ff}(\boldsymbol{x}) = & -\frac{\cos\theta}{2\pi|\boldsymbol{x}|^2} \int_{\Gamma_p} \left(\begin{bmatrix} 0 \\ 0 \\ 1 \end{bmatrix} \cdot \boldsymbol{n}_{\boldsymbol{y}}\, \mu(\boldsymbol{y}) - y_3 \nu(\boldsymbol{y}) \right) \mathrm{d}\gamma(\boldsymbol{y}) \\ & + i\, e^{-i\pi/4} \sqrt{\frac{Z_\infty}{2\pi|\boldsymbol{x}_s|}}\, e^{-Z_\infty x_3} e^{iZ_\infty |\boldsymbol{x}_s|} \\ & \int_{\Gamma_p} e^{-Z_\infty y_3} e^{-iZ_\infty \boldsymbol{y}_s \cdot \hat{\boldsymbol{x}}_s} \left(Z_\infty \begin{bmatrix} \cos\varphi \\ \sin\varphi \\ 1 \end{bmatrix} \cdot \boldsymbol{n}_{\boldsymbol{y}}\, \mu(\boldsymbol{y}) + \nu(\boldsymbol{y}) \right) \mathrm{d}\gamma(\boldsymbol{y}). \end{aligned} \tag{4.190}$$

The asymptotic behavior of the solution u at infinity, as $|\boldsymbol{x}| \to \infty$, is therefore given by

$$u(\boldsymbol{x}) = \frac{1}{|\boldsymbol{x}|^2}\left\{u_\infty^A(\hat{\boldsymbol{x}}) + \mathcal{O}\left(\frac{1}{|\boldsymbol{x}|}\right)\right\} + \frac{e^{-Z_\infty x_3} e^{iZ_\infty|\boldsymbol{x}_s|}}{\sqrt{|\boldsymbol{x}_s|}}\left\{u_\infty^S(\hat{\boldsymbol{x}}_s) + \mathcal{O}\left(\frac{1}{|\boldsymbol{x}_s|}\right)\right\}, \quad (4.191)$$

where we decompose $\boldsymbol{x} = |\boldsymbol{x}|\,\hat{\boldsymbol{x}}$, being $\hat{\boldsymbol{x}} = (\sin\theta\cos\varphi, \sin\theta\sin\varphi, \cos\theta)$ a vector of the unit sphere, and $\boldsymbol{x}_s = |\boldsymbol{x}_s|\,\hat{\boldsymbol{x}}_s$, being $\hat{\boldsymbol{x}}_s = (\cos\varphi, \sin\varphi)$ a vector of the unit circle. The far-field pattern of the asymptotic decaying is given by

$$u_\infty^A(\hat{\boldsymbol{x}}) = -\frac{\cos\theta}{2\pi}\int_{\Gamma_p}\left(\begin{bmatrix}0\\0\\1\end{bmatrix}\cdot\boldsymbol{n}_{\boldsymbol{y}}\,\mu(\boldsymbol{y}) - y_3\nu(\boldsymbol{y})\right)\mathrm{d}\gamma(\boldsymbol{y}), \quad (4.192)$$

whereas the far-field pattern for the surface waves adopts the form

$$u_\infty^S(\hat{\boldsymbol{x}}_s) = \frac{iZ_\infty^{1/2}}{\sqrt{2\pi}}\,e^{-i\pi/4}\int_{\Gamma_p} e^{-Z_\infty y_3} e^{-iZ_\infty \boldsymbol{y}_s\cdot\hat{\boldsymbol{x}}_s}\left(Z_\infty\begin{bmatrix}\cos\varphi\\\sin\varphi\\1\end{bmatrix}\cdot\boldsymbol{n}_{\boldsymbol{y}}\,\mu(\boldsymbol{y}) + \nu(\boldsymbol{y})\right)\mathrm{d}\gamma(\boldsymbol{y}). \quad (4.193)$$

Both far-field patterns can be expressed in decibels (dB) respectively by means of the scattering cross sections

$$Q_s^A(\hat{\boldsymbol{x}})\ \ [\text{dB}] = 20\log_{10}\left(\frac{|u_\infty^A(\hat{\boldsymbol{x}})|}{|u_0^A|}\right), \quad (4.194)$$

$$Q_s^S(\hat{\boldsymbol{x}}_s)\ \ [\text{dB}] = 20\log_{10}\left(\frac{|u_\infty^S(\hat{\boldsymbol{x}}_s)|}{|u_0^S|}\right), \quad (4.195)$$

where the reference levels u_0^A and u_0^S are taken such that $|u_0^A| = |u_0^S| = 1$ if the incident field is given by a surface wave of the form (4.15).

We remark that the far-field behavior (4.191) of the solution is in accordance with the radiation condition (4.6), which justifies its choice.

4.8 Existence and uniqueness

4.8.1 Function spaces

To state a precise mathematical formulation of the herein treated problems, we have to define properly the involved function spaces. Since the considered domains and boundaries are unbounded, we need to work with weighted Sobolev spaces, as in Durán, Muga & Nédélec (2005*b*, 2009). We consider the classic weight functions

$$\varrho = \sqrt{1+r^2} \qquad \text{and} \qquad \log\varrho = \ln(2+r^2), \quad (4.196)$$

where $r = |\boldsymbol{x}|$. We define the domains

$$\Omega_e^1 = \left\{\boldsymbol{x}\in\Omega_e :\ x_3 > \frac{1}{2Z_\infty}\ln\big(1+2\pi Z_\infty r^3\big),\right\}, \quad (4.197)$$

$$\Omega_e^2 = \left\{\boldsymbol{x}\in\Omega_e :\ x_3 < \frac{1}{2Z_\infty}\ln\big(1+2\pi Z_\infty r^3\big),\right\}. \quad (4.198)$$

It holds that the solution of the direct scattering problem (4.13) is contained in the weighted Sobolev space

$$W^1(\Omega_e) = \left\{ v : \frac{v}{\varrho} \in L^2(\Omega_e),\ \nabla v \in L^2(\Omega_e)^2,\ \frac{v}{\sqrt{\varrho}} \in L^2(\Omega_e^1),\ \frac{\partial v}{\partial r} \in L^2(\Omega_e^1), \right.$$
$$\left. \frac{v}{\log \varrho} \in L^2(\Omega_e^2),\ \frac{1}{\log \varrho}\left(\frac{\partial v}{\partial r} - iZ_\infty v\right) \in L^2(\Omega_e^2) \right\}. \tag{4.199}$$

With the appropriate norm, the space $W^1(\Omega_e)$ becomes also a Hilbert space. We have likewise the inclusion $W^1(\Omega_e) \subset H^1_{\text{loc}}(\Omega_e)$, i.e., the functions of these two spaces differ only by their behavior at infinity.

Since we are dealing with Sobolev spaces, even a strong Lipschitz boundary $\Gamma \in C^{0,1}$ is admissible. The fact that this boundary Γ is also unbounded implies that we have to use weighted trace spaces like in Amrouche (2002). For this purpose, we consider the space

$$W^{1/2}(\Gamma) = \left\{ v :\ \frac{v}{\sqrt{\varrho}\log \varrho} \in H^{1/2}(\Gamma) \right\}. \tag{4.200}$$

Its dual space $W^{-1/2}(\Gamma)$ is defined via W^0-duality, i.e., considering the pivot space

$$W^0(\Gamma) = \left\{ v :\ \frac{v}{\sqrt{\varrho}\log \varrho} \in L^2(\Gamma) \right\}. \tag{4.201}$$

Analogously as for the trace theorem (A.531), if $v \in W^1(\Omega_e)$ then the trace of v fulfills

$$\gamma_0 v = v|_\Gamma \in W^{1/2}(\Gamma). \tag{4.202}$$

Moreover, the trace of the normal derivative can be also defined, and it holds that

$$\gamma_1 v = \frac{\partial v}{\partial n}|_\Gamma \in W^{-1/2}(\Gamma). \tag{4.203}$$

We remark further that the restriction of the trace of v to Γ_p is such that

$$\gamma_0 v|_{\Gamma_p} = v|_{\Gamma_p} \in H^{1/2}(\Gamma_p), \tag{4.204}$$

$$\gamma_1 v|_{\Gamma_p} = \frac{\partial v}{\partial n}|_{\Gamma_p} \in H^{-1/2}(\Gamma_p), \tag{4.205}$$

and its restriction to Γ_∞ yields

$$\gamma_0 v|_{\Gamma_\infty} = v|_{\Gamma_\infty} \in W^{1/2}(\Gamma_\infty), \tag{4.206}$$

$$\gamma_1 v|_{\Gamma_\infty} = \frac{\partial v}{\partial n}|_{\Gamma_\infty} \in W^{-1/2}(\Gamma_\infty). \tag{4.207}$$

4.8.2 Application to the integral equation

The existence and uniqueness of the solution for the direct scattering problem (4.13), due the integral representation formula (4.174), can be characterized by using the integral equation (4.185). For this purpose and in accordance with the considered function spaces, we take $\mu \in H^{1/2}(\Gamma_p)$ and $\nu \in H^{-1/2}(\Gamma_p)$. Furthermore, we consider that $Z \in L^\infty(\Gamma_p)$ and that $f_z \in H^{-1/2}(\Gamma_p)$, even though strictly speaking $f_z \in \widetilde{H}^{-1/2}(\Gamma_p)$.

It holds that the single and double layer potentials defined respectively in (4.176) and (4.177) are linear and continuous integral operators such that

$$\mathcal{S} : H^{-1/2}(\Gamma_p) \longrightarrow W^1(\Omega_e) \qquad \text{and} \qquad \mathcal{D} : H^{1/2}(\Gamma_p) \longrightarrow W^1(\Omega_e). \tag{4.208}$$

The boundary integral operators (4.183) and (4.184) are also linear and continuous applications, and they are such that

$$S : H^{-1/2}(\Gamma_p) \longrightarrow W^{1/2}(\Gamma) \qquad \text{and} \qquad D : H^{1/2}(\Gamma_p) \longrightarrow W^{1/2}(\Gamma). \tag{4.209}$$

When we restrict them to Γ_p, then it holds that

$$S|_{\Gamma_p} : H^{-1/2}(\Gamma_p) \longrightarrow H^{1/2}(\Gamma_p) \qquad \text{and} \qquad D|_{\Gamma_p} : H^{1/2}(\Gamma_p) \longrightarrow H^{1/2}(\Gamma_p). \tag{4.210}$$

Let us consider the integral equation (4.185), which is given in terms of boundary layer potentials, for $\mu \in H^{1/2}(\Gamma_p)$, by

$$(1 + \mathcal{I}_0)\frac{\mu}{2} + S(Z\mu) - D(\mu) = S(f_z) \qquad \text{in } \ H^{1/2}(\Gamma_p). \tag{4.211}$$

Due the imbedding properties of Sobolev spaces and in the same way as for the half-plane impedance Laplace problem, it holds that the left-hand side of the integral equation corresponds to an identity and two compact operators, and thus Fredholm's alternative holds.

Since the Fredholm alternative applies to the integral equation, therefore it applies also to the direct scattering problem (4.13) due the integral representation formula. The existence of the scattering problem's solution is thus determined by its uniqueness, and the values for the impedance $Z \in \mathbb{C}$ for which the uniqueness is lost constitute a countable set, which we call the impedance spectrum of the scattering problem and denote it by σ_Z. The existence and uniqueness of the solution is therefore ensured almost everywhere. The same holds obviously for the solution of the integral equation, whose impedance spectrum we denote by ς_Z. Since the integral equation is derived from the scattering problem, it holds that $\sigma_Z \subset \varsigma_Z$. The converse, though, is not necessarily true. In any way, the set $\varsigma_Z \setminus \sigma_Z$ is at most countable. In conclusion, the scattering problem (4.13) admits a unique solution u if $Z \notin \sigma_Z$, and the integral equation (4.185) admits a unique solution μ if $Z \notin \varsigma_Z$.

4.9 Dissipative problem

The dissipative problem considers surface waves that lose their amplitude as they travel along the half-space's boundary. These waves dissipate their energy as they propagate and are modeled by a complex impedance $Z_\infty \in \mathbb{C}$ whose imaginary part is strictly positive, i.e., $\mathfrak{Im}\{Z_\infty\} > 0$. This choice ensures that the surface waves of the Green's function (4.113) decrease exponentially at infinity. Due the dissipative nature of the medium, it is no longer suited to take progressive plane surface waves in the form of (4.15) as the incident field u_I. Instead, we have to take a source of surface waves at a finite distance from the perturbation. For example, we can consider a point source located at $\boldsymbol{z} \in \Omega_e$, in which case the incident field is given, up to a multiplicative constant, by

$$u_I(\boldsymbol{x}) = G(\boldsymbol{x}, \boldsymbol{z}), \tag{4.212}$$

where G denotes the Green's function (4.113). This incident field u_I satisfies the Laplace equation with a source term in the right-hand side, namely

$$\Delta u_I = \delta_{\boldsymbol{z}} \qquad \text{in } \mathcal{D}'(\Omega_e), \tag{4.213}$$

which holds also for the total field u_T but not for the scattered field u, in which case the Laplace equation remains homogeneous. For a general source distribution g_s, whose support is contained in Ω_e, the incident field can be expressed by

$$u_I(\boldsymbol{x}) = G(\boldsymbol{x}, \boldsymbol{z}) * g_s(\boldsymbol{z}) = \int_{\Omega_e} G(\boldsymbol{x}, \boldsymbol{z})\, g_s(\boldsymbol{z})\, \mathrm{d}\boldsymbol{z}. \tag{4.214}$$

This incident field u_I satisfies now

$$\Delta u_I = g_s \qquad \text{in } \mathcal{D}'(\Omega_e), \tag{4.215}$$

which holds again also for the total field u_T but not for the scattered field u.

It is not difficult to see that all the performed developments for the non-dissipative case are still valid when considering dissipation. The only difference is that now a complex impedance Z_∞ such that $\mathfrak{Im}\{Z_\infty\} > 0$ has to be taken everywhere into account.

4.10 Variational formulation

To solve the integral equation we convert it to its variational or weak formulation, i.e., we solve it with respect to a certain test function in a bilinear (or sesquilinear) form. Basically, the integral equation is multiplied by the (conjugated) test function and then the equation is integrated over the boundary of the domain. The test function is taken in the same function space as the solution of the integral equation.

The variational formulation for the integral equation (4.211) searches $\mu \in H^{1/2}(\Gamma_p)$ such that $\forall \varphi \in H^{1/2}(\Gamma_p)$ we have that

$$\left\langle (1 + \mathcal{I}_0)\frac{\mu}{2} + S(Z\mu) - D(\mu), \varphi \right\rangle = \left\langle S(f_z), \varphi \right\rangle. \tag{4.216}$$

4.11 Numerical discretization

4.11.1 Discretized function spaces

The scattering problem (4.13) is solved numerically with the boundary element method by employing a Galerkin scheme on the variational formulation of the integral equation. We use on the boundary surface Γ_p Lagrange finite elements of type $\mathbb{P}_1$. The surface Γ_p is approximated by the triangular mesh Γ_p^h, composed by T flat triangles T_j, for $1 \leq j \leq T$, and I nodes $\boldsymbol{r}_i \in \mathbb{R}^3$, $1 \leq i \leq I$. The triangles have a diameter less or equal than h, and their vertices or corners, i.e., the nodes $\boldsymbol{r}_i$, are on top of Γ_p, as shown in Figure 4.10. The diameter of a triangle K is given by

$$\mathrm{diam}(K) = \sup_{\boldsymbol{x},\boldsymbol{y} \in K} |\boldsymbol{y} - \boldsymbol{x}|. \tag{4.217}$$

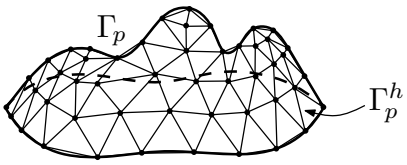

FIGURE 4.10. Mesh Γ_p^h, discretization of Γ_p.

The function space $H^{1/2}(\Gamma_p)$ is approximated using the conformal space of continuous piecewise linear polynomials with complex coefficients

$$Q_h = \big\{\varphi_h \in C^0(\Gamma_p^h) \,:\, \varphi_h|_{T_j} \in \mathbb{P}_1(\mathbb{C}),\;\; 1 \le j \le T\big\}. \tag{4.218}$$

The space Q_h has a finite dimension I, and we describe it using the standard base functions for finite elements of type $\mathbb{P}_1$, which we denote by $\{\chi_j\}_{j=1}^I$. The base function χ_j is associated with the node $\boldsymbol{r}_j$ and has its support $\operatorname{supp}\chi_j$ on the triangles that have $\boldsymbol{r}_j$ as one of their vertices. On $\boldsymbol{r}_j$ it has a value of one and on the opposed edges of the triangles its value is zero, being linearly interpolated in between and zero otherwise.

In virtue of this discretization, any function $\varphi_h \in Q_h$ can be expressed as a linear combination of the elements of the base, namely

$$\varphi_h(\boldsymbol{x}) = \sum_{j=1}^{I} \varphi_j\, \chi_j(\boldsymbol{x}) \qquad \text{for } \; \boldsymbol{x} \in \Gamma_p^h, \tag{4.219}$$

where $\varphi_j \in \mathbb{C}$ for $1 \le j \le I$. The solution $\mu \in H^{1/2}(\Gamma_p)$ of the variational formulation (4.216) can be therefore approximated by

$$\mu_h(\boldsymbol{x}) = \sum_{j=1}^{I} \mu_j\, \chi_j(\boldsymbol{x}) \qquad \text{for } \; \boldsymbol{x} \in \Gamma_p^h, \tag{4.220}$$

where $\mu_j \in \mathbb{C}$ for $1 \le j \le I$. The function f_z can be also approximated by

$$f_z^h(\boldsymbol{x}) = \sum_{j=1}^{I} f_j\, \chi_j(\boldsymbol{x}) \qquad \text{for } \; \boldsymbol{x} \in \Gamma_p^h, \quad \text{with } \; f_j = f_z(\boldsymbol{r}_j). \tag{4.221}$$

4.11.2 Discretized integral equation

To see how the boundary element method operates, we apply it to the variational formulation (4.216). We characterize all the discrete approximations by the index h, including also the impedance and the boundary layer potentials. The numerical approximation of (4.216) leads to the discretized problem that searches $\mu_h \in Q_h$ such that $\forall \varphi_h \in Q_h$

$$\Big\langle (1 + \mathcal{I}_0^h)\frac{\mu_h}{2} + S_h(Z_h\mu_h) - D_h(\mu_h), \varphi_h \Big\rangle = \big\langle S_h(f_z^h), \varphi_h \big\rangle. \tag{4.222}$$

Considering the decomposition of μ_h in terms of the base $\{\chi_j\}$ and taking as test functions the same base functions, $\varphi_h = \chi_i$ for $1 \leq i \leq I$, yields the discrete linear system

$$\sum_{j=1}^{I} \mu_j \left(\frac{1}{2} \big\langle (1 + \mathcal{I}_0^h)\chi_j, \chi_i \big\rangle + \langle S_h(Z_h\chi_j), \chi_i \rangle - \langle D_h(\chi_j), \chi_i \rangle \right) = \sum_{j=1}^{I} f_j \, \langle S_h(\chi_j), \chi_i \rangle. \tag{4.223}$$

This constitutes a system of linear equations that can be expressed as a linear matrix system:

$$\begin{cases} \text{Find } \boldsymbol{\mu} \in \mathbb{C}^I \text{ such that} \\ \boldsymbol{M}\boldsymbol{\mu} = \boldsymbol{b}. \end{cases} \tag{4.224}$$

The elements m_{ij} of the matrix $\boldsymbol{M}$ are given, for $1 \leq i, j \leq I$, by

$$m_{ij} = \frac{1}{2} \big\langle (1 + \mathcal{I}_0^h)\chi_j, \chi_i \big\rangle + \langle S_h(Z_h\chi_j), \chi_i \rangle - \langle D_h(\chi_j), \chi_i \rangle, \tag{4.225}$$

and the elements b_i of the vector $\boldsymbol{b}$ by

$$b_i = \big\langle S_h(f_z^h), \chi_i \big\rangle = \sum_{j=1}^{I} f_j \, \langle S_h(\chi_j), \chi_i \rangle \qquad \text{for } \; 1 \leq i \leq I. \tag{4.226}$$

The discretized solution u_h, which approximates u, is finally obtained by discretizing the integral representation formula (4.174) according to

$$u_h = \mathcal{D}_h(\mu_h) - \mathcal{S}_h(Z_h\mu_h) + \mathcal{S}_h(f_z^h), \tag{4.227}$$

which, more specifically, can be expressed as

$$u_h = \sum_{j=1}^{I} \mu_j \big(\mathcal{D}_h(\chi_j) - \mathcal{S}_h(Z_h\chi_j) \big) + \sum_{j=1}^{I} f_j \, \mathcal{S}_h(\chi_j). \tag{4.228}$$

We remark that the resulting matrix $\boldsymbol{M}$ is in general complex, full, non-symmetric, and with dimensions $I \times I$. The right-hand side vector $\boldsymbol{b}$ is complex and of size I. The boundary element calculations required to compute numerically the elements of $\boldsymbol{M}$ and $\boldsymbol{b}$ have to be performed carefully, since the integrals that appear become singular when the involved segments are adjacent or coincident, due the singularity of the Green's function at its source point. On Γ_0, the singularity of the image source point has to be taken additionally into account for these calculations.

4.12 Boundary element calculations

The boundary element calculations build the elements of the matrix $\boldsymbol{M}$ resulting from the discretization of the integral equation, i.e., from (4.224). They permit thus to compute numerically expressions like (4.225). To evaluate the appearing singular integrals, we adapt the semi-numerical methods described in the report of Bendali & Devys (1986).

We use the same notation as in Section D.12, and the required boundary element integrals, for $a, b \in \{0, 1\}$ and $c, d \in \{1, 2, 3\}$, are again

$$ZA_{a,b}^{c,d} = \int_K \int_L \left(\frac{s_c}{h_c^K}\right)^a \left(\frac{t_d}{h_d^L}\right)^b G(\boldsymbol{x}, \boldsymbol{y}) \, \mathrm{d}L(\boldsymbol{y}) \, \mathrm{d}K(\boldsymbol{x}), \tag{4.229}$$

$$ZB_{a,b}^{c,d} = \int_K \int_L \left(\frac{s_c}{h_c^K}\right)^a \left(\frac{t_d}{h_d^L}\right)^b \frac{\partial G}{\partial n_{\boldsymbol{y}}}(\boldsymbol{x}, \boldsymbol{y}) \, \mathrm{d}L(\boldsymbol{y}) \, \mathrm{d}K(\boldsymbol{x}). \tag{4.230}$$

All the integrals that stem from the numerical discretization can be expressed in terms of these two basic boundary element integrals. The impedance is again discretized as a piecewise constant function Z_h, which on each triangle T_j adopts a constant value $Z_j \in \mathbb{C}$. The integrals of interest are the same as for the full-space impedance Laplace problem and we consider furthermore that

$$\left\langle (1 + \mathcal{I}_0^h)\chi_j, \chi_i \right\rangle = \begin{cases} \langle \chi_j, \chi_i \rangle & \text{if } \boldsymbol{r}_j \in \Gamma_+, \\ 2 \langle \chi_j, \chi_i \rangle & \text{if } \boldsymbol{r}_j \in \Gamma_0. \end{cases} \tag{4.231}$$

To compute the boundary element integrals (4.229) and (4.230), we can easily isolate the singular part (4.119) of the Green's function (4.113), which corresponds in fact to the Green's function of the Laplace equation in the full-space, and therefore the associated integrals are computed in the same way. The same applies also for its normal derivative. In the case when the triangles K and L are are close enough, e.g., adjacent or coincident, and when $L \in \Gamma_0^h$ or $K \in \Gamma_0^h$, being Γ_0^h the approximation of Γ_0, we have to consider additionally the singular behavior (4.120), which is linked with the presence of the impedance half-space. This behavior can be straightforwardly evaluated by replacing $\boldsymbol{x}$ by $\bar{\boldsymbol{x}}$ in formulae (D.295) to (D.298), i.e., by computing the quantities $ZF_b^d(\bar{\boldsymbol{x}})$ and $ZG_b^d(\bar{\boldsymbol{x}})$ with the corresponding adjustment of the notation. Otherwise, if the triangles are not close enough and for the non-singular part of the Green's function, a three-point Gauss-Lobatto quadrature formula is used. All the other computations are performed in the same manner as in Section D.12 for the full-space Laplace equation.

4.13 Benchmark problem

As benchmark problem we consider the particular case when the domain $\Omega_e \subset \mathbb{R}^3_+$ is taken as the exterior of a half-sphere of radius $R > 0$ that is centered at the origin, as shown in Figure 4.11. We decompose the boundary of Ω_e as $\Gamma = \Gamma_p \cup \Gamma_\infty$, where Γ_p corresponds to the upper half-sphere, whereas Γ_∞ denotes the remaining unperturbed portion of the half-space's boundary which lies outside the half-sphere and which extends towards infinity. The unit normal $\boldsymbol{n}$ is taken outwardly oriented of Ω_e, e.g., $\boldsymbol{n} = -\boldsymbol{r}$ on Γ_p.

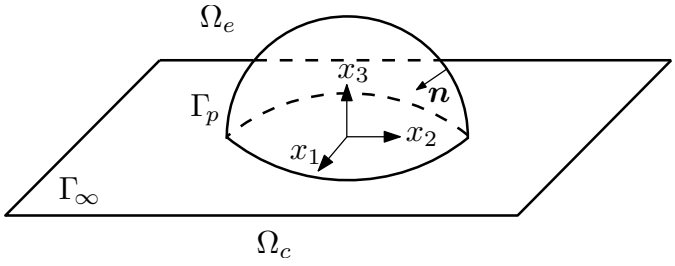

FIGURE 4.11. Exterior of the half-sphere.

The benchmark problem is then stated as

$$\begin{cases} \text{Find } u : \Omega_e \to \mathbb{C} \text{ such that} \\ \Delta u = 0 & \text{in } \Omega_e, \\ -\dfrac{\partial u}{\partial n} + Zu = f_z & \text{on } \Gamma, \\ \text{+ Outgoing radiation condition as } |\boldsymbol{x}| \to \infty, \end{cases} \tag{4.232}$$

where we consider a constant impedance $Z \in \mathbb{C}$ throughout Γ and where the radiation condition is as usual given by (4.6). As incident field u_I we consider the same Green's function, namely

$$u_I(\boldsymbol{x}) = G(\boldsymbol{x}, \boldsymbol{z}), \tag{4.233}$$

where $\boldsymbol{z} \in \Omega_c$ denotes the source point of our incident field. The impedance data function f_z is hence given by

$$f_z(\boldsymbol{x}) = \frac{\partial G}{\partial n_{\boldsymbol{x}}}(\boldsymbol{x}, \boldsymbol{z}) - ZG(\boldsymbol{x}, \boldsymbol{z}), \tag{4.234}$$

and its support is contained in Γ_p. The analytic solution for the benchmark problem (4.232) is then clearly given by

$$u(\boldsymbol{x}) = -G(\boldsymbol{x}, \boldsymbol{z}). \tag{4.235}$$

The goal is to retrieve this solution numerically with the integral equation techniques and the boundary element method described throughout this chapter.

For the computational implementation and the numerical resolution of the benchmark problem, we consider integral equation (4.185). The linear system (4.224) resulting from the discretization (4.222) of its variational formulation (4.216) is solved computationally with finite boundary elements of type $\mathbb{P}_1$ by using subroutines programmed in Fortran 90, by generating the mesh Γ_p^h of the boundary with the free software Gmsh 2.4, and by representing graphically the results in Matlab 7.5 (R2007b).

We consider a radius $R = 1$, a constant impedance $Z = 5$, and for the incident field a source point $\boldsymbol{z} = (0, 0, 0)$. The discretized perturbed boundary curve Γ_p^h has $I = 641$ nodes, $T = 1224$ triangles and a discretization step $h = 0.1676$, being

$$h = \max_{1 \le j \le T} \operatorname{diam}(T_j). \tag{4.236}$$

The numerically calculated trace of the solution μ_h of the benchmark problem, which was computed by using the boundary element method, is depicted in Figure 4.12. In the same manner, the numerical solution u_h is illustrated in Figures 4.13 and 4.14 for an angle $\varphi = 0$. It can be observed that the numerical solution is close to the exact one.

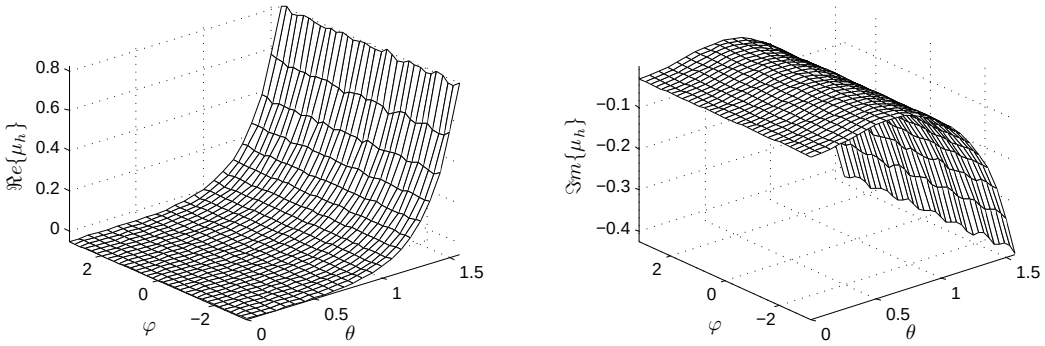

(a) Real part (b) Imaginary part

FIGURE 4.12. Numerically computed trace of the solution μ_h.

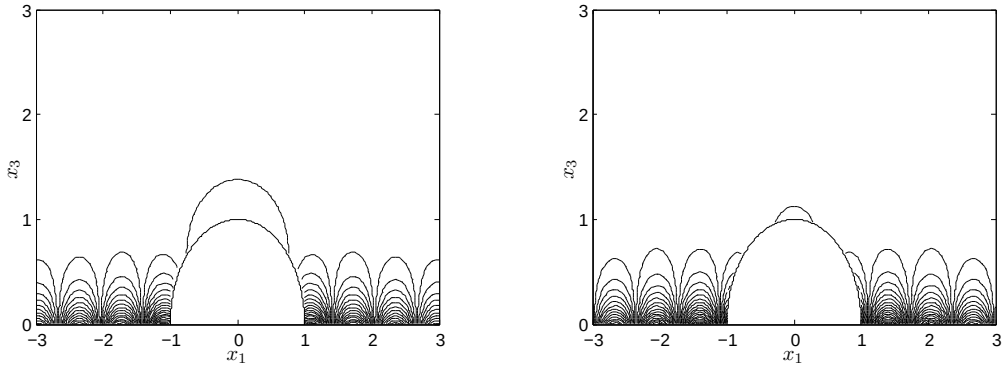

(a) Real part (b) Imaginary part

FIGURE 4.13. Contour plot of the numerically computed solution u_h for $\varphi = 0$.

Likewise as in (D.346), we define the relative error of the trace of the solution as

$$E_2(h, \Gamma_p^h) = \frac{\|\Pi_h \mu - \mu_h\|_{L^2(\Gamma_p^h)}}{\|\Pi_h \mu\|_{L^2(\Gamma_p^h)}}, \tag{4.237}$$

where $\Pi_h \mu$ denotes the Lagrange interpolating function of the exact solution's trace μ, i.e.,

$$\Pi_h \mu(\boldsymbol{x}) = \sum_{j=1}^{I} \mu(\boldsymbol{r}_j)\, \chi_j(\boldsymbol{x}) \quad \text{and} \quad \mu_h(\boldsymbol{x}) = \sum_{j=1}^{I} \mu_j\, \chi_j(\boldsymbol{x}) \quad \text{for } \boldsymbol{x} \in \Gamma_p^h. \tag{4.238}$$

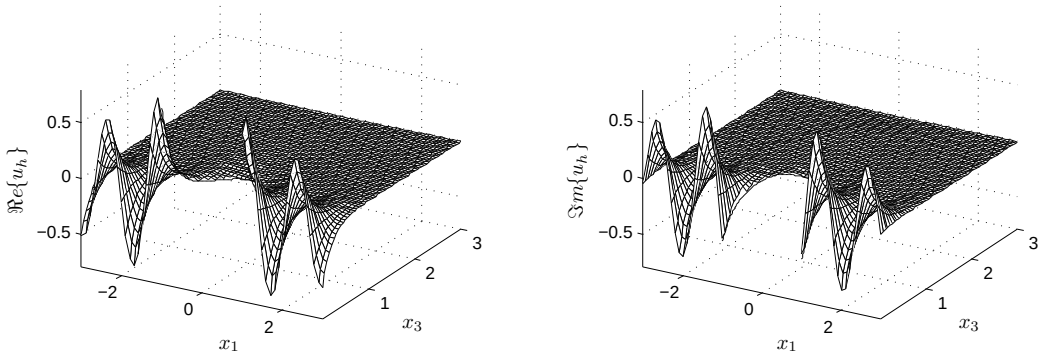

(a) Real part (b) Imaginary part

FIGURE 4.14. Oblique view of the numerically computed solution u_h for $\varphi = 0$.

In our case, for a step $h = 0.1676$, we obtained a relative error of $E_2(h, \Gamma_p^h) = 0.05359$.

As in (D.350), we define the relative error of the solution as

$$E_\infty(h, \Omega_L) = \frac{\|u - u_h\|_{L^\infty(\Omega_L)}}{\|u\|_{L^\infty(\Omega_L)}}, \tag{4.239}$$

being $\Omega_L = \{\boldsymbol{x} \in \Omega_e : \|\boldsymbol{x}\|_\infty < L\}$ for $L > 0$. We consider $L = 3$ and approximate Ω_L by a triangular finite element mesh of refinement h near the boundary. For $h = 0.1676$, the relative error that we obtained for the solution was $E_\infty(h, \Omega_L) = 0.05509$.

The results for different mesh refinements, i.e., for different numbers of triangles T, nodes I, and discretization steps h for Γ_p^h, are listed in Table 4.1. These results are illustrated graphically in Figure 4.15. It can be observed that the relative errors are approximately of order h^2.

TABLE 4.1. Relative errors for different mesh refinements.

T	I	h	$E_2(h, \Gamma_p^h)$	$E_\infty(h, \Omega_L)$
46	30	0.7071	$2.863 \cdot 10^{+1}$	$4.582 \cdot 10^{+1}$
168	95	0.4320	$3.096 \cdot 10^{-1}$	$4.131 \cdot 10^{-1}$
466	252	0.2455	$1.233 \cdot 10^{-1}$	$1.373 \cdot 10^{-1}$
700	373	0.1987	$8.414 \cdot 10^{-2}$	$9.262 \cdot 10^{-2}$
1224	641	0.1676	$5.359 \cdot 10^{-2}$	$5.509 \cdot 10^{-2}$
2100	1090	0.1286	$3.182 \cdot 10^{-2}$	$4.890 \cdot 10^{-2}$

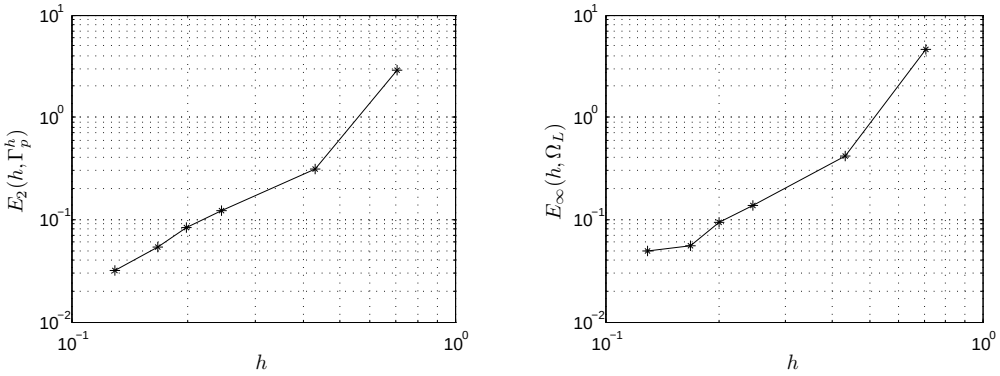

(a) Relative error $E_2(h, \Gamma_p^h)$ (b) Relative error $E_\infty(h, \Omega_L)$

FIGURE 4.15. Logarithmic plots of the relative errors versus the discretization step.